UCRL-20376
c. 2

NUCLEAR RELAXATION IN NICKEL ALLOYS

Boris Chornik
(Ph. D. Thesis)

December 1970

AEC Contract No. W-7405-eng-48

UCRL-20376 c. 2

LAWRENCE RADIATION LABORATORY
UNIVERSITY of CALIFORNIA BERKELEY

DISCLAIMER

Contents

ABSTRACT ---------- v

I. INTRODUCTION ---------- 1

II. NUCLEAR SPIN-LATTICE RELAXATION ---------- 6

A. General Formulas ---------- 7

B. Contact Relaxation ---------- 14

C. Orbital Relaxation ---------- 16

D. Dipolar Relaxation ---------- 22

E. Other Mechanisms ---------- 25

III. EXPERIMENT ---------- 28

A. Apparatus ---------- 28

B. Sample Preparation ---------- 34

C. Results ---------- 36

IV. INTERPRETATION OF RESULTS ---------- 43

A. Nickel Relaxation ---------- 43

B. Palladium Relaxation ---------- 47

C. Description of the Impurity State ---------- 48

D. Discussion ---------- 52

V. SUMMARY AND CONCLUSIONS ---------- 58

ACKNOWLEDGMENTS ---------- 60

REFERENCES ---------- 61

APPENDIX ---------- 65

TABLES ---------- 73

FIGURE CAPTIONS ---------- 75

FIGURES ---------- 77

may be heat, static magnetic or electric fields, alternating electromagnetic fields, or a combination of several of them. This seems to be simple but, in most cases, it becomes very complex. Take for instance a nuclear magnetic resonance experiment. Here, the stimulation is a static magnetic field plus an electromagnetic field (which may be cw or pulsed). The response is the resonant absorption of rf power, and the modification of the nuclear magnetization. We may look at a steady-state and a transient response (spin-lattice relaxation, spin-spin relaxation). Both may be measured as functions of temperature and static magnetic field.

A very fruitful approach in the study of metals has been to add an impurity and study the physical properties of the host metal and the impurity. Both are modified in the alloy with respect to the original constituents. In some cases, the observed effects are a consequence of the change in electron concentration of the electronic bands. For instance, the measurement of the saturation magnetization of alloys of the ferromagnetic metals with other transition metals shows that the impurity, as a first approximation, simply contributes with extra electrons or holes (according to its valence). This contribution adds or subtracts from the host magnetization. The variation is linear, as can be seen in the Slater-Pauling diagram.[2] This is confirmed by the measurement of the electronic specific heat.[3]

In some cases, an impurity may develop a magnetic moment, even if the host is non-magnetic. This surprising phenomenon has been observed in magnetic susceptibility measurements[4,5] (where a temperature-dependent term appears), neutron scattering experiments,[6] or measurements

of the hyperfine field at the nuclear site.[7] The most widely-used methods to measure the latter are nuclear magnetic resonance,[8] Mössbauer effect,[9] measurement of the nuclear specific heat,[10] and perturbed angular correlation.[11] Here we have mentioned only representative samples of a literature that covers a very wide field of research. The local moments are produced by an interaction of the impurity d-levels with the host conduction electrons.[12-14] Several transport effects occur as a consequence of this interaction. For instance, Kondo[15] calculated the scattering cross section of conduction electrons up to second order and was able to explain the well-known minimum of resistivity as a function of temperature for certain alloys. It has been predicted[16] that sometimes a quasi-bound state is formed between the localized moment and the conduction electrons.

In ferromagnetic hosts it is interesting to know the magnetization distribution around the impurity. The most direct way is by neutron scattering experiments;[17,18] however, in cases of very dilute alloys neutron diffraction may not yield observable results and one has to get more indirect evidence by the other methods, e.g. by measuring the hyperfine field. However, the disadvantage of these methods is that their interpretation is somewhat ambiguous due to the several contributions with either sign which sometimes almost cancel. Our experiment serves this purpose: it gives information about the impurity state. Its advantage is that interpretation is very simple, as we shall see later.

The nuclear spin-lattice relaxation experiment consists of a) applying an rf field at the nuclear Larmor frequency in order to change

the equilibrium distribution of the Zeeman levels, or in other words, to increase the nuclear spin temperature, b) turning off the rf field and monitoring the recovery of the longitudinal nuclear magnetization (by the spin echo technique[19]). This shows the thermal contact between the nuclear spins and the lattice. Usually the recovery is an exponential function of time, and one can define a relaxation time T_1 so that:

$$M_z = M_o [1-\exp(-t/T_1)]$$

where M_z is the z-nuclear magnetization and M_o its equilibrium value.

There are several mechanisms for the nuclear relaxation; all of them involve electrons in some way or another. In metals, the most important mechanisms are due to direct electron scattering, so that the relaxation time T_1 varies inversely with temperature. We shall see in the second chapter that in the case of transition metals, the dominant process is a nuclear spin-electron orbital moment interaction to d electrons. We shall see also that our measurement gives the density of states of d electrons in the vicinity of the nucleus, and that this result can provide indirect information on the magnetic moment distribution around the impurity. Such a study was made by Bancroft[20] in the case of Ni-Cu alloys. He found that there is no localized magnetic moment on the Cu impurity.

The second chapter is devoted to a theoretical study of the relaxation process in metals, with special emphasis on transition metals, i.e. metals with a non-vanishing d density of states at the Fermi surface.

The third chapter describes the experiment in detail: the apparatus, the sample preparation, and the results.

The fourth chapter gives an interpretation of the experimental results. The value of the Pd magnetic moment is calculated. A discussion follows in order to relate this conclusion to other experimental facts and also to describe the impurity state of Pd in Ni.

Finally, we would like to explain why we chose Pd as an impurity to add to Ni metal. It is known that the Pd metal electronic structure is very similar to that of Ni metal and that Pd is easily polarizable, due to exchange effects. Therefore we would expect a behavior qualitatively different to that of the Cu impurity in Ni. Besides, Pd is under Ni in the periodic table, so that the valence is the same. Therefore, we would not expect screening effects, a fact that simplifies the theoretical interpretation.

II. NUCLEAR SPIN - LATTICE RELAXATION

Korringa[21] made the first calculation of the nuclear spin-lattice relaxation rate in metals through interactions between the nuclear spins and the conduction electrons. Comparisons between these theoretical calculations and the experimental results are quite good for simple metals, where conduction electrons belong to s and p states and all other states of d of f symmetry are either completely filled or completely empty. The agreement is good, provided that electron-electron interactions effects are considered.[22] The agreement is poor for transition metals. It was found by Obata[23] that in these cases the partly filled d-bands contribute to the relaxation with a new mechanism. His calculation shows that this new mechanism is much more important than the normal interaction with conduction electrons. Later, Moriya[24] took into account all the possible mechanisms in the particular case of the ferromagnetic metals nickel, iron and cobalt, to get a relaxation rate that would agree fairly well with experimental data.

This chapter presents a detailed treatment of the nuclear spin-lattice relaxation rate, based on the above mentioned papers by Korringa, Obata and Moriya. Complete derivation of the formulas are given. They are not usually found in the literature. We believe a thesis is the appropriate place to report them. It is always necessary, because sometimes numerical errors appear and someone must check them. For instance, an error of a factor of four was found by Walsted, Jaccarino and Kaplan[25] in Moriya's paper.

A. General Formulas

The interaction responsible for the nuclear relaxation in metals is produced by the fluctuating magnetic field felt by the nuclei and caused by the electron spins and the orbital motion of the electrons. For the electron spins we have two cases to consider: the contact interaction, for electrons with no angular momentum (s-electrons), and the dipolar interaction, for electrons with non-zero angular momentum. Of course, orbital interaction exists only for electrons with non-zero angular momentum. The expressions for the various interactions are the following:

Contact interaction: $$\mathcal{H}^{c} = \frac{8\pi}{3} \gamma_e \gamma_n \hbar^2 \delta(\underline{r})\, \underline{I}\cdot\underline{S} \qquad (1)$$

Orbital interaction: $$\mathcal{H}^{orb} = \gamma_e \gamma_n \hbar^2 r^{-3}\, \underline{I}\cdot\underline{L} \qquad (2)$$

Dipolar interaction: $$\mathcal{H}^{dip} = \gamma_e \gamma_n \hbar^2 r^{-5}[3(\underline{r}\cdot\underline{S})(\underline{I}\cdot\underline{r}) - r^2 \underline{I}\cdot\underline{S}] \qquad (3)$$

where γ_e and γ_n are the electronic and nuclear gyromagnetic ratios, $\underline{I}$ is the nuclear spin, $\underline{S}$ is the electron spin, $\underline{L}$ is the electronic angular momentum and $\underline{r}$ is the radius vector between the nucleus and the electron.

It is convenient to re-write the above expressions in terms of the raising and lowering operators, $I_{\pm} = I_x \pm iI_y$, etc. We get:

$$\mathcal{H}^{c} = \frac{8\pi}{3} \gamma_e \gamma_n \hbar^2 \delta(r) \cdot \left(\frac{1}{2} I_+ S_- + \frac{1}{2} I_- S_+ + I_z S_z\right)$$

$$\mathcal{H}^{orb} = \gamma_e \gamma_n \hbar^2 r^{-3} \left(\frac{1}{2} I_+ L_- + \frac{1}{2} I_- L_+ + I_z L_z\right)$$

$$\begin{aligned}\mathcal{H}^{dip} = \gamma_e \gamma_n \hbar^2 r^{-3} \{ & I_+ \left[\frac{3x_-^2}{4r^2} S_+ + \frac{3x_+x_-}{4r^2} S_- + \frac{3zx_-}{2r^2} S_z - \frac{1}{2} S_-\right] \\ & + I_- \left[\frac{3x_+x_-}{4r^2} S_+ + \frac{3x_+^2}{4r^2} S_- + \frac{3zx_+}{2r^2} S_z - \frac{1}{2} S_+\right] \\ & + I_z \left[\frac{3zx_-}{2r^2} S_+ + \frac{3zx_+}{2r^2} S_- + \frac{3z^2}{r^2} S_z - S_z\right]\}\end{aligned}$$

So that in general we can write the interaction hamiltonian as follows:

$$\mathcal{H} = I_+\Phi_- + I_-\Phi_+ + I_z\Phi_z \tag{4}$$

where

$$\Phi_\pm^c = \frac{8\pi}{3}\gamma_e\gamma_n\hbar^2\delta(\underline{r})\cdot\frac{1}{2}S_\pm \tag{5a}$$

$$\Phi_z^c = \frac{8\pi}{3}\gamma_e\gamma_n\hbar^2\delta(\underline{r})\cdot S_z \tag{5b}$$

$$\Phi_\pm^{orb} = \gamma_e\gamma_n\hbar^2 r^{-3}\frac{1}{2}L_\pm \tag{6a}$$

$$\Phi_z^{orb} = \gamma_e\gamma_n\hbar^2 r^{-3}L_z \tag{6b}$$

$$\Phi_\pm^{dip} = \gamma_e\gamma_n\hbar^2 r^{-3}\frac{1}{2}\left\{\left(\frac{3}{2}\frac{x_+x_-}{r^2}-1\right)S_\pm + \frac{3}{2}\frac{x_\pm^2}{r^2}S_\mp + \frac{3zx_\pm}{r^2}S_z\right\} \tag{7a}$$

$$\Phi_z^{dip} = \gamma_e\gamma_n\hbar^2 r^{-3}\left\{\left(\frac{3z^2}{r^2}-1\right)S_z + \frac{3}{2}\frac{zx_-}{r^2}S_+ + \frac{3}{2}\frac{zx_+}{r^2}S_-\right\} \tag{7b}$$

The relaxation process is treated as a time-dependent first order perturbation by the above interactions. We start with an initial state $|m\underline{k}\sigma\rangle$ where m labels the nuclear Zeeman state, $\underline{k}$ is the electron wave vector and σ its spin. The final state, after scattering of the electron by the nucleus, is $|m'\underline{k}'\sigma'\rangle$. We can see by inspection that whenever the nuclear spin flips, the electronic spin or the angular momentum flips in the opposite direction, so that the total angular momentum is conserved, as it must. The matrix elements are:

$$\langle m\underline{k}\sigma|\mathcal{H}|m'\underline{k}'\sigma'\rangle = \langle m|I_-|m'\rangle\langle\underline{k}\sigma|\Phi_+|\underline{k}'\sigma'\rangle + \langle m|I_+|m'\rangle\langle\underline{k}\sigma|\Phi_-|k'\sigma'\rangle.$$

We have neglected the term in $I_z\Phi_z$ since $\langle m|I_z|m'\rangle = 0$ for $m \neq m'$ and we are interested only in transitions where there is a change in Zeeman energy.

Now the transition probability $W_{mm'}$, between two nuclear states is given by the Golden Rule:

$$W_{mm'} = \frac{2\pi}{\hbar} \sum_{\substack{\underline{k}\,\underline{k}' \\ \sigma\,\sigma'}} |\langle m\underline{k}\sigma|\mathcal{H}|m'\underline{k}'\sigma'\rangle|^2 \delta(E_{m\underline{k}\sigma}-E_{m'\underline{k}'\sigma'})f(E_{\underline{k}\sigma})[1-f(E_{\underline{k}'\sigma'})] \tag{8}$$

where $E_{k\sigma}$ is the electron energy and $f(E)$ is the Fermi distribution function,

$$f(E) = \{1 + \exp[(E-E_f)/k_BT]\}^{-1}.$$

In order to define and calculate the spin-lattice relaxation time T_1 we must assume that the spins are in thermal equilibrium among themselves, due to spin-spin interactions. This equilibrium is described by a spin temperature T_S, so that there is a Boltzmann distribution of the population of spins at the different nuclear Zeeman levels. If $P_m^{(S)}$ is the probability of occupancy of a state at energy E_m, then:

$$P_m^{(S)} = \frac{1}{Z}\exp(-E_m\beta_S) \tag{9}$$

where $\beta_S = (k_BT_S)^{-1}$ and Z is the partition function

$$Z^{(S)} = \sum_m \exp(-E_m\beta_S). \tag{10}$$

The spin temperature T_S is equal to the lattice temperature T at equilibrium. We alter this equilibrium by irradiation of the sample with an electromagnetic field that induces transitions between the Zeeman levels. After this perturbation, the spins reach an equilibrium

at a new spin temperature T_S that is different than the lattice temperature T. This happens within a time T_2 (the so-called spin-spin relaxation time) after suppressing the perturbation. Later, T_S approaches T due to the spin-lattice interaction. We shall see that T_S follows the differential equation:

$$\frac{d\beta_S}{dt} = \frac{1}{T_1} (\beta-\beta_S) \tag{11}$$

which defines the spin-lattice relaxation time T_1. Here, $\beta = (k_B T)^{-1}$.

We start with the so-called "master" equation:

$$\frac{d}{dt} P_m^{(S)} = \sum_{m'} (P_{m'}^{(S)} W_{m'm} - P_m^{(S)} W_{mm'})$$

which relates the rate of change of the Boltzmann probabilities to the transition probabilities. Next, we evaluate the average energy of the spin system, $\bar{E}$, and see how it changes:

$$\bar{E} = \sum_m P_m^{(S)} E_m \tag{12}$$

$$\frac{d\bar{E}}{dt} = \sum_m E_m \frac{d}{dt} P_m^{(S)}$$

$$= \sum_{m,m'} (P_m^{(S)} W_{mm'} - P_{m'}^{(S)} W_{m'm}) E_{m'}$$

$$= \frac{1}{2} \sum_{m,m'} (P_m^{(S)} W_{mm'} - P_{m'}^{(S)} W_{m'm})(E_{m'} - E_m) \tag{13}$$

On the other hand, we can write that

$$\frac{d\bar{E}}{dt} = \frac{d\beta_S}{dt} \frac{d\bar{E}}{d\beta_S} \tag{14}$$

From (12) we get the equation

$$\frac{d\bar{E}}{d\beta_S} = \frac{d}{d\beta_S} \sum_m P_m^{(S)} E_m$$

$$= \sum_m E_m \frac{d}{d\beta_S} P_m^{(S)} \tag{15}$$

From (9) we have:

$$\frac{d}{d\beta_S} P_m^{(S)} = - \frac{E_m}{Z^{(S)}} \exp(-E_m\beta_S) - \frac{1}{Z^{(S)2}} \exp(-E_m\beta_S) \frac{dZ^{(S)}}{d\beta_S} \tag{16}$$

We can expand (10) in the high-temperature approximation, $E_m\beta_S << 1$

$$Z^{(S)} = \sum_m (1 - \beta_S E_m + \frac{1}{2!} \beta_S^2 E_m^2 - \cdots)$$

$$= Z_o + \left(-\beta_S \sum_m E_m + \frac{1}{2!} \beta_S^2 \sum_m E_m^2 - \cdots \right)$$

where $Z_o = 2I + 1$. Now the term in β_S can be made equal to zero with a suitable choice of the representation and the following terms are negligible in the high-temperature approximation, so that

$$Z^{(S)} \approx Z_o = 2I + 1$$

$$\frac{dZ^{(S)}}{d\beta_S} = 0$$

Introducing these results in (16) we get:

$$\frac{d}{d\beta_S} P_m^{(S)} = \frac{-E_m}{Z_o}$$

So that equation (15) leads to:

$$\frac{d\bar{E}}{d\beta_S} = - \frac{1}{Z_o} \sum_m E_m^2$$

From (14):

$$\frac{d\bar{E}}{dt} = - \frac{1}{Z_o} \frac{d\beta_S}{dt} \sum_m E_m^2 \qquad (17)$$

By comparison of (13) and (17) we get

$$\frac{d\beta_S}{dt} \sum_m E_m^2 = \frac{Z_o}{2} \sum_{m,m'} [P_m^{(S)} W_{mm'} - P_{m'}^{(S)} W_{m'm}](E_m - E_{m'}) \qquad (18)$$

Now we shall introduce the lattice temperature T and the corresponding populations P_m. By the principle of the detailed balance, at equilibrium each term in the sum of equation (18) vanishes so that:

$$P_m W_{mm'} = P_{m'} W_{m'm}$$

Hence:

$$\frac{d\beta_S}{dt} \sum_m E_m^2 = \frac{Z_o}{2} \sum_{m,m'} P_m^{(S)} W_{mm'} \left[1 - \frac{P_{m'}^{(S)}}{P_{m'}} \frac{P_m}{P_m^{(S)}} \right] (E_m - E_{m'})$$

By replacing $P_m^{(S)} \approx \frac{1}{Z_o}$ and expanding the exponential, we get:

$$\frac{d\beta_S}{dt} \sum_m E_m^2 = \frac{1}{2} (\beta - \beta_S) \sum_{mm'} W_{mm'} (E_m - E_{m'})^2$$

This differential equation for β_S is of the expected form (11). The relaxation time T_1 is given by:

$$\frac{1}{T_1} = \frac{1}{2} \frac{\sum_{mm'} W_{mm'}(E_m - E_{m'})^2}{\sum_m E_m} \tag{19}$$

Equation (19) is the so called "Gorter's formula". Its derivation is found in most textbooks on magnetic resonance, like Slichter's, Abragam's, etc. We included it here for the sake of completeness.

Now we return to equation (8). The total energy difference between initial and final state is:

$$E_{m\underline{k}\sigma} - E_{m'\underline{k}'\sigma'} = E_{\underline{k}\sigma} - E_{\underline{k}'\sigma'} \pm \hbar\omega$$

where ω is the Larmor frequency of the nuclear spins. The Zeeman energy can be neglected here since it is very small in comparison with the electronic energies. Also, because of the δ-function, we can replace $E_{\underline{k}'\sigma'}$ by $E_{\underline{k}\sigma}$ and get:

$$f(E_{\underline{k}\sigma})[1 - f(E_{\underline{k}\sigma})] \simeq k_B T \delta(E_{\underline{k}\sigma} - E_F)$$

where E_F is the Fermi energy and k_B is the Boltzmann constant. Thus, the transition probability is:

$$W_{mm'} = \frac{2\pi}{\hbar} k_B T \sum_{\substack{\underline{k} \\ \sigma}} \sum_{\substack{\underline{k}' \\ \sigma'}} |\langle m\underline{k}\sigma|\mathcal{H}|m'\underline{k}'\sigma'\rangle|^2 \delta(E_{\underline{k}\sigma} - E_{\underline{k}'\sigma'}) \, \delta(E_{\underline{k}\sigma} - E_F) \tag{20}$$

The transition probability $W_{mm'}$ turns out to be proportional to the temperature, a fact characteristic of direct processes of scattering.

B. Contact Relaxation

From now on, we have to specify the type of interaction and the wave functions. Let us take first the contact interaction (5a). The wave functions are given by the following Bloch functions:

$$|m\underline{k}\sigma\rangle = |m\rangle|\sigma\rangle\ u_{\underline{k}\sigma}(\underline{r})\ \exp\ (i\underline{k}\cdot\underline{r}) \tag{21}$$

where $u_{\underline{k}}(\underline{r})$ has the lattice symmetry. Then:

$$\langle m\underline{k}\sigma|\mathcal{H}^c|m'\underline{k}'\sigma'\rangle = \langle m|I_+|m'\rangle\ \langle \underline{k}\sigma|\Phi^c_-|k'\sigma'\rangle + \langle m|I_-|m'\rangle\langle \underline{k}\sigma|\Phi^c_+|\underline{k}'\sigma'\rangle$$

Using (5a) and (21)

$$\langle \underline{k}\sigma|\Phi^c_\pm|\underline{k}'\sigma'\rangle = \frac{8\pi}{3}\gamma_e\gamma_n\hbar^2\,\frac{1}{2}\int d^3r\delta(\underline{r})\ \exp\ [i(\underline{k}-\underline{k}')\cdot\underline{r}]u_{\underline{k}\sigma}(r)\ u^*_{\underline{k}'\sigma'}(r)$$

$$\times\ \langle\sigma|S_\pm|\sigma'\rangle$$

$$\langle k\sigma|\Phi^c_\pm|k'\sigma'\rangle = \frac{8\pi}{3}\gamma_e\gamma_n\hbar^2\,\frac{1}{2}\,u_{k\sigma}(0)u^*_{k'\sigma'}(0)\ \langle\sigma|S_\pm|\sigma'\rangle$$

$$W^c_{mm'} = \frac{2\pi}{\hbar}\,k_B T\left(\frac{8\pi}{3}\gamma_e\gamma_n\hbar^2\right)^2\cdot\frac{1}{2}\,\langle|u_\uparrow(0)|^2\rangle_F\ \langle|u_\downarrow(0)|^2\rangle_F$$

$$\times\ N^s_\uparrow(E_F)\times N^s_\downarrow(E_F)\times|\langle m|I_+ + I_-|m'\rangle|^2$$

where the arrows indicate the electron spin direction, $N^s_\uparrow(E_F)$ is the density of states per atom of spin up s-electrons at the Fermi level, and correspondently, $N^s_\downarrow(E_F)$ is the density of states of spin down s-electrons.

Now, the matrix elements between the nuclear states are zero unless $m' = m+1$. In this case,

$$\langle m|I_+ + I_-|m\pm1\rangle = \sqrt{I(I+1) - m(m\pm1)}$$

Hence we can write the transition probability in the form:

$$W^c_{mm\pm1} = W^c_o \left[I(I+1) - m(m\pm1)\right]$$

where:

$$W^c_o = \frac{32}{9}\pi^3\hbar^3 k_B T \gamma_e^2\gamma_n^2 \left\langle|u_\uparrow(0)|^2\right\rangle_F \cdot \left\langle|u_\downarrow(0)|^2\right\rangle_F \times N^s_\uparrow(E_F) \cdot N^s_\downarrow(E_F)$$

Note that if we have a nucleus with spin I = 1/2, then W^c_o is the probability of a transition from m = 1/2 to m = -1/2.

Now we replace the expressions for $W_{mm'}$ and $E_m = -m\hbar\omega$ in formula (19) to get the relaxation time T^c_1:

$$\frac{1}{T^c_1} = \frac{\sum_m W_{mm+1}(\hbar\omega)^2 + \sum_m W_{mm-1}(\hbar\omega)^2}{2\sum_m m^2(\hbar\omega)^2}$$

$$\frac{1}{T^c_1} = \frac{W^c_o}{2}\frac{\sum_m [I(I+1) - m(m+1)] + \sum_m [I(I+1) - m(m-1)]}{\sum_m^{m^2}}$$

From the relation $\sum_{m=-J}^{m=I} m^2 = \frac{I(2I+1)(I+1)}{3}$ we get:

$$\frac{1}{T^c_1} = 2W^c_o$$

The relaxation time T^c_1 turns out to be independent of the nuclear spin I, and it is equal to twice the transition rate corresponding to spin 1/2. In general,

$$\frac{1}{T_1} = 2W_o \tag{22}$$

where: $$W_o = \frac{2\pi}{\hbar} k_B T \sum_{\substack{\underline{k}\,\underline{k}'\\ \sigma\,\sigma'}} \left|\langle \underline{k}\sigma|\Phi_+|\underline{k}'\sigma'\rangle\right|^2 \delta(E_{\underline{k}\sigma} - E_{\underline{k}'\sigma'})\, \delta(E_{\underline{k}\sigma} - E_F) \tag{23}$$

Since we are interested in the electronic contribution to the relaxation process, it is useful to define a relaxation rate R that is independent of the temperature and the characteristics of the nucleus involved, in the following way:

$$R = (\gamma_n^2 T_1 T)^{-1}$$

so that we finally get

$$R^c = \frac{64}{9}\,\pi^3 \hbar^3 k_B \gamma_e^2 \,\langle |u_\uparrow(0)|^2 \rangle_F \,\langle |u_\downarrow(0)|^2 \rangle_F \, N_\uparrow^s(E_F)\, N_\downarrow^s(E_F) \qquad (24)$$

For the common case of a non-polarized s-band where

$$N_\uparrow^s(E_F) = N_\downarrow^s(E_F) = N^s(E_F)/2 \text{ and } u_\uparrow^s(0) = u_\downarrow^s(0) = u^s(0)$$

we have

$$R^c = \frac{16}{9}\,\pi^3 \hbar^3 k_B \gamma_e^2 \,\langle |u^s(0)|^2 \rangle_F^2 \,[N^s(E_F)]^2 \qquad (25)$$

C. Orbital Relaxation

It is more difficult to derive the dipolar and orbital relaxation rates in a closed form, like the contact relaxation. For non-zero angular momentum states, the tight-binding approximation is generally used. It is simple enough to render soluble equations. In spite of its failure to describe itinerant effects, the results are reasonably accurate here because the relaxation process occurs in the local vicinity of the nucleus, where the electronic wavefunctions have essentially an atomic character. To define the wavefunctions, we must specify an additional band index μ:

$$|\mu \underline{k} \sigma\rangle = N^{-1/2} \sum_{\underline{R}} \exp(i\underline{k}\cdot\underline{R}) \sum_n u_{\mu n \underline{k} \sigma} \; |\phi_n(\underline{r}-\underline{R})\rangle |\sigma\rangle \qquad (26)$$

where N is the total number of atoms in the crystal, $\underline{R}$ is the position vector of any nucleus and $\phi_n(\underline{r})$ is an atomic wave function.

As we are interested in nickel, we will make the calculation for d-wavefunctions, since it is known that in Ni the 3d band has a high density of states at the Fermi surface, and this parameter appears as a multiplicative factor in the relaxation rate (as we shall see later).

The atomic d-functions ϕ_n are five-fold degenerate in the free atom; the levels are split when placing the atom in the cubic crystal field. We get two-fold degenerate levels that transform according to Γ_3 irreducible representation and three-fold degenerate levels that correspond to Γ_5, the latter having the higher energy. We will take the ϕ_n's as the basis for these representations. They are written as linear combinations of the spherical harmonics $Y_{2,m}(\theta,\phi)$ multiplied by a m-independent radial function, as follows:

$$\phi_1(\underline{r}) = \sqrt{\frac{15}{4\pi}}\,\frac{xy}{r^2}\,f(r) = \frac{i}{\sqrt{2}}\,[Y_{2,-2}(\theta,\phi) - Y_{2,2}(\theta,\phi)]\,f(r)$$

$$\phi_2(\underline{r}) = \sqrt{\frac{15}{4\pi}}\,\frac{yz}{r^2}\,f(r) = \frac{i}{\sqrt{2}}\,[Y_{2,1}(\theta,\phi) - Y_{2,-1}(\theta,\phi)]\,f(r)$$

$$\phi_3(\underline{r}) = \sqrt{\frac{15}{4\pi}}\,\frac{zx}{r^2}\,f(r) = \frac{1}{\sqrt{2}}\,[Y_{2,1}(\theta,\phi) + Y_{2,-1}(\theta,\phi)]\,f(r) \qquad (27)$$

$$\phi_4(\underline{r}) = \sqrt{\frac{15}{16\pi}}\,\frac{(x^2-y^2)}{r^2}\,f(r) = \frac{1}{\sqrt{2}}\,[Y_{2,2}(\theta,\phi) + Y_{2,-2}(\theta,\phi)]\,f(r)$$

$$\phi_5(\underline{r}) = \sqrt{\frac{15}{16\pi}}\,\frac{(3z^2-r^2)}{r^2}\,f(r) = Y_{2,0}(\theta,\phi)\,f(r).$$

Our wavefunctions $|\mu\underline{k}\sigma\rangle$ are linear combinations of L.C.A.O. wavefunctions, with coefficients $u_{\mu n\underline{k}\sigma}$. All these coefficients are thus the matrix elements of a unitary transformation from the L.C.A.O. wavefunctions.

The following orthogonality conditions are fulfilled:

$$\sum_{\mu} u^{*}_{\mu n \underline{k}\sigma}\, u_{\mu n' \underline{k}\sigma} = \delta_{nn'}$$

$$\sum_{n} u^{*}_{\mu n \underline{k}\sigma}\, u_{\mu' n \underline{k}\sigma} = \delta_{\mu\mu'} \qquad (28)$$

The relaxation time is obtained by replacing (26) and (27) in (23):

$$W_o^{orb} = \frac{2\pi}{\hbar}\, k_B T \sum_{\substack{\underline{k}\\ \sigma}} \sum_{\substack{\underline{k}'\\ \sigma'}} \sum_{\substack{\mu\mu'\\ \underline{R}}} \left| \langle \mu \underline{k}\sigma | \Phi_+^{orb} | \mu' \underline{k}'\sigma' \rangle \right|^2 \delta(E_{\mu \underline{k}\sigma} - E_{\mu' \underline{k}'\sigma'}) \delta(E_{\mu \underline{k}\sigma} - E_F)$$

Taking matrix elements between wavefunctions of the same atom, we have

$$\langle \mu \underline{k}\sigma | \Phi_+^{orb} | \mu' \underline{k}'\sigma' \rangle = N^{-1} \sum_{\underline{R}} \exp[i(\underline{k}-\underline{k}')\cdot \underline{R}] \sum_{n_1 n_1'} u_{\mu n_1 \underline{k}\sigma} u^{*}_{\mu' n_1' \underline{k}'\sigma'} \delta_{\sigma\sigma'}$$

$$\times \langle \phi_{n_1}(\underline{r}-\underline{R}) | \Phi_+^{orb} | \phi_{n_1'}(\underline{r}-\underline{R}) \rangle$$

$$\left| \langle \mu \underline{k}\sigma | \Phi_+^{orb} | \mu' \underline{k}'\sigma' \rangle \right|^2 = N^{-1} \delta_{\sigma\sigma'} \sum_{\substack{n_1 n_1'\\ n_2 n_2'}} u_{\mu n_1 \underline{k}\sigma} u^{*}_{\mu' n_1' \underline{k}'\sigma'} u^{*}_{\mu n_2 \underline{k}\sigma} u_{\mu' n_2' \underline{k}'\sigma'}$$

$$\times \langle \phi_{n_1} | \Phi_+^{orb} | \phi_{n_1'} \rangle \langle \phi_{n_2'} | \Phi_-^{orb} | \phi_{n_2} \rangle$$

Hence

$$W_o^{orb} = \frac{2\pi}{\hbar} k_B T \sum_{\substack{\underline{k}\,\underline{k}' \\ \sigma\,\sigma'}} \sum_{\mu\mu'} \sum_{\substack{n_1 n_1' \\ n_2 n_2'}} \delta_{\sigma\sigma'} u_{\mu n_1 \underline{k}\sigma} u^*_{\mu_1' n_1' k'\sigma'} u^*_{\mu n_2 \underline{k}\sigma} u_{\mu' n_2' \underline{k}'\sigma'}$$

$$\times \langle \phi_{n_1} | \Phi_+^{orb} | \phi_{n_1'} \rangle \langle \phi_{n_2'} | \Phi_-^{orb} | \phi_{n_2} \rangle \; \delta(E_{\mu\underline{k}\sigma} - E_{\mu\underline{k}'\sigma'}) \delta(E_{\mu\underline{k}\sigma} - E_F)$$

The next step is to define average values of $|u_{\mu n\underline{k}\sigma}|^2$ taken at a surface of constant energy E:

$$C_{n\sigma}(E) = \langle |u_{\mu n\underline{k}\sigma}|^2 \rangle$$

$$= \sum_{\mu\underline{k}} |u_{\mu n\underline{k}\sigma}|^2 \delta(E_{\mu\underline{k}\sigma} - E) \; / N_\sigma^d(E)$$

where $N_\sigma^d(E)$ is the density of states at energy E for states of spin σ only.

Using the sum rule:

$$\sum_{\mu\underline{k}} u_{\mu n\underline{k}\sigma} u^*_{\mu n'\underline{k}\sigma} \delta(E_{\mu\underline{k}\sigma} - E) = \delta_{nn'} N_\sigma^d(E) \; C_{n\sigma}(E) \qquad (29)$$

we can simplify the expression for W_o^{orb} to get:

$$W_o^{orb} = \frac{2\pi}{\hbar} k_B T \sum_{\underline{k}\sigma} \sum_{\mu} \sum_{\substack{n_1 n_1' \\ n_2}} u_{\mu n_1 \underline{k}\sigma} u_{\mu n_2 \underline{k}\sigma} \langle \phi_{n_1} | \Phi_+^{orb} | \phi_{n_1'} \rangle$$

$$\times \langle \phi_{n_1'} | \Phi_-^{orb} | \phi_{n_2} \rangle \delta(E_{\mu \underline{k}\sigma} - E_F) N_\sigma^d(E_F) C_{n_1'\sigma}(E_F)$$

$$W_o^{orb} = \frac{2\pi}{\hbar} k_B T \sum_{\sigma} \sum_{n_1 n_1'} |\langle \phi_{n_1} | \Phi_+^{orb} | \phi_{n_1'} \rangle|^2 [N_\sigma^d(E_F)]^2 C_{n_1\sigma}(E_F) C_{n_1'\sigma}(E_F) \qquad (30)$$

The matrix element of $\Phi_+^{orb} = \gamma_e \gamma_n \hbar^2 r^{-3} \frac{1}{2} L_+$ are calculated using the equation

$$L_+ Y_{2,m}(\theta,\phi) = \sqrt{6-m(m+1)}\, Y_{2,m+1}(\theta,\phi).$$

$$L_+ = \begin{bmatrix} 0 & 1 & -i & 0 & 0 \\ 1 & 0 & 0 & -i & i\sqrt{3} \\ i & 0 & 0 & 1 & \sqrt{3} \\ 0 & i & 1 & 0 & 0 \\ 0 & -i\sqrt{3} & \sqrt{3} & 0 & 0 \end{bmatrix}$$

Hence, $\langle \phi_n | \Phi_+^{orb} | \phi_{n'} \rangle = \gamma_e \gamma_n \hbar^2 \frac{1}{2} \langle n | L_+ | n' \rangle \int r^{-3} f^2(r) r^2 dr$

Defining $$\langle r^{-3} \rangle = \int r^{-3} f^2(r) r^2 dr$$

Then: $\langle \phi_n | \Phi_+^{orb} | \phi_{n'} \rangle = \gamma_e \gamma_n \hbar^2 \frac{1}{2} \langle r^{-3} \rangle \langle n | L_+ | n' \rangle$

Before evaluating the summation, we can see that the coefficients $C_{n\sigma}$ are related. From (29):

$$\sum_{\mu n \underline{k}} |u_{\mu n \underline{k}\sigma}|^2 \delta(E_{\mu \underline{k}\sigma} - E) = N_\sigma^d(E) \sum_n C_{n\sigma}(E)$$

Employing (28), we get:

$$\sum_{\mu \underline{k}} \delta(E_{\mu \underline{k}\sigma} - E) = N_\sigma^d(E) \sum_n C_{n\sigma}(E)$$

Hence: $\sum_n C_{n\sigma}(E) = 1.$

Due to the degeneracy within each manifold, the coefficient $C_{n\sigma}$ is the same for all the wavefunctions corresponding to the same irreducible representation (Γ_5 or Γ_3). Let us define:

$$C_{1\sigma} = C_{2\sigma} = C_{3\sigma} = \frac{1}{3} f_\sigma$$

$$C_{4\sigma} = C_{5\sigma} = \frac{1}{2} - \frac{1}{2} f_\sigma$$

Replacing in (30) the value of the matrix elements and the coefficients $C_{n\sigma}$'s, we get

$$W_o^{orb} = \frac{2\pi}{3\hbar} k_B T (\gamma_e \gamma_n \hbar^2)^2 \langle r^{-3} \rangle^2 \sum_\sigma [N_\sigma^d(E_F)]^2 f_\sigma (2 - \frac{5}{3} f_\sigma)$$

$$\frac{1}{T_1^{orb}} = \frac{4\pi}{3\hbar} k_B T (\gamma_e \gamma_n \hbar^2)^2 \langle r^{-3} \rangle^2 \sum_\sigma [N_\sigma^d(E_F)]^2 f_\sigma (2 - \frac{5}{3} f_\sigma)$$

$$R^{orb} = \frac{4\pi}{3} \hbar^3 k_B \gamma_e^2 \langle r^{-3} \rangle^2 \sum_\sigma [N_\sigma^d(E_F)]^2 f_\sigma (2 - \frac{5}{3} f_\sigma) \qquad (31)$$

D. Dipolar Relaxation

Here we employ again the same representation used for the orbital calculation. Following the same steps, we get the equation

$$W_o^{dip} = \frac{2\pi}{\hbar} k_B T \sum_{\sigma\sigma'} \sum_{nn'} |\langle \phi_n \sigma | \Phi_+^{dip} | \phi_n \sigma' | \phi_n \sigma' \rangle|^2 N_\sigma^d(E_F) N_{\sigma'}^d(E_F) C_{n\sigma}(E_F) C_{n'\sigma'}(E_F)$$

The expression (7a) has to be rewritten in terms of polar coordinates and then in terms of spherical harmonics:

$$\Phi_+^{dip} = \gamma_e \gamma_n \hbar^2 r^{-3} \frac{1}{2}\{(\frac{3}{2}\sin^2\theta - 1)S_+ + \frac{3}{2}\sin^2\theta e^{2i\phi} S_- + 3\sin\theta\cos\theta e^{i\phi} S_z\}$$

$$\Phi_+^{dip} = \gamma_e \gamma_n \hbar^2 r^{-3} \left\{ -\sqrt{\frac{\pi}{5}} Y_{2,0}(\theta,\phi) S_+ + \sqrt{\frac{6\pi}{5}} Y_{2,2}(\theta,\phi) S_- - \sqrt{\frac{6\pi}{5}} Y_{2,2}(\theta\ \phi) S_z \right\}$$

Calculation of the matrix elements involves evaluation of integrals of the form:

$$\int Y^*_{2,m_1}(\theta,\phi) Y_{2,m_2}(\theta,\phi) Y_{2,m_3}(\theta,\phi) d\Omega$$

By substituting the $Y_{2,m}$'s in terms of the associated Legendre polynomials we can see that the integral vanishes unless $m_1 = m_2 + m_3$. If this condition is fulfilled, the integral has a value given in Table I. Calculations were made after direct substitution of each associated Legendre polynomial, as function of $X = \cos\theta$. Another way (suggested by Rose[26]) is to use the formula:

$$\int Y^*_{\ell_3 m_3} Y_{\ell_2 m_2} Y_{\ell_1 m_1} d\Omega = \sqrt{\frac{(2\ell_1+1)(2\ell_2+1)}{4\pi(2\ell_3+1)}}\ C(\ell_1\ell_2\ell_3; m_1 m_2 m_3) C(\ell_1\ell_2\ell_3; 000)$$

where the C's are Clebsch-Gordan coefficients. These are tabulated, for instance, by Condon and Shortley.[27]

The results can be presented in the form:

$$\Phi_{+}^{dip} = \gamma_e \gamma_n \hbar^2 r^{-3} (M_+ S_+ + M_- S_- + M_z S_z)$$

$$M_+ = \begin{bmatrix} 1/7 & 0 & 0 & 0 & 0 \\ 0 & -1/14 & 0 & 0 & 0 \\ 0 & 0 & -1/14 & 0 & 0 \\ 0 & 0 & 0 & 1/7 & 0 \\ 0 & 0 & 0 & 0 & -1/7 \end{bmatrix}$$

$$M_- = \begin{bmatrix} 0 & 0 & 0 & 0 & \sqrt{3}i/7 \\ 0 & -3/14 & 3i/14 & 0 & 0 \\ 0 & -3i/14 & 3/14 & 0 & 0 \\ 0 & 0 & 0 & 0 & -\sqrt{3}/7 \\ -\sqrt{3}i/7 & 0 & 0 & -\sqrt{3}/7 & 0 \end{bmatrix}$$

$$M_z = \begin{bmatrix} 0 & 3/14 & -3i/14 & 0 & 0 \\ 3/14 & 0 & 0 & 3i/14 & -\sqrt{3}i/14 \\ -3i/14 & 0 & 0 & -3/14 & -\sqrt{3}/14 \\ 0 & -3i/14 & -3/14 & 0 & 0 \\ 0 & \sqrt{3}i/14 & -\sqrt{3}/14 & 0 & 0 \end{bmatrix}$$

Hence,

$$W_o^{dip} = \frac{2\pi}{\hbar} k_B T(\gamma_e\gamma_n\hbar^2)^2 \langle r^{-3}\rangle^2 \sum_{\sigma\sigma'}\sum_{nn'} N_\sigma^d(N_F)N_{\sigma'}^d(E_F)$$

$$\times C_{n\sigma}(E_F)C_{n'\sigma'}(E_F)\left[|\langle\phi_n|M_+|\phi_{n'}\rangle|^2|\langle\sigma|S_+|\sigma'\rangle|^2 + \right.$$

$$\left. |\langle\phi_n|M_-|\phi_{n'}\rangle|^2|\langle\sigma|S_-|\sigma'\rangle|^2 + |\langle\phi_n|M_z|\phi_{n'}\rangle|^2|\langle\sigma|S_z|\sigma'\rangle|^2\right]$$

$$W_o^{dip} = \frac{2\pi}{\hbar} k_B T(\gamma_e\gamma_n\hbar^2)^2 \langle r^{-3}\rangle^2 \sum_{nn'}\left\{N_\uparrow^d(E_F)N_\downarrow^d(E_F)C_{n\uparrow}C_{n'\downarrow}(E_F)\right.$$

$$\times\left[|\langle\phi_n|M_+|\phi_{n'}\rangle|^2 + |\langle\phi_n|M_-|\phi_{n'}\rangle|^2\right] + \frac{1}{4}\sum_\sigma [N_\sigma^d(E_F)]^2 C_{n\sigma}(E_F)$$

$$\left.\times C_{n'\sigma}(E_F)|\langle\phi_n|M_z|\phi_{n'}\rangle|^2\right\}$$

Substitution of the values of the C's and the matrix elements gives

$$W_o^{dip} = \frac{2\pi}{\hbar} k_B T(\gamma_e\gamma_n\hbar^2)^2 \langle r^{-3}\rangle^2 \frac{1}{196}\left\{N_\uparrow^d(E_F)N_\downarrow^d(E_F)\right.$$

$$\left.\times\left(\frac{26}{3} f_\uparrow f_\downarrow - 6f_\uparrow - 6f_\downarrow + 8\right) + \sum_\sigma [N_\sigma^d(E_F)]^2 f_\sigma(2-f_\sigma)\right\}$$

$$R^{dip} = \frac{4\pi}{3}\hbar^3 k_B \gamma_e^2 \langle r^{-3}\rangle^2 \frac{1}{196}\left\{2N_\uparrow^d(E_F)N_\downarrow^d(E_F)(13f_\uparrow f_\downarrow - 9f_\uparrow - 9f_\downarrow + 12)\right.$$

$$\left. + \sum_\sigma 3[N_\sigma^d(E_F)]^2 f_\sigma(2-f_\sigma)\right\} \qquad (32)$$

We can see that the dipolar relaxation rate has two terms: one that comes from processes in which the electronic spin flips and the other one from processes where the electronic spin does not change (but the

orbital angular momentum does). The first part vanishes in situations where the d-band is polarized and one sub-band lies entirely below the Fermi energy. If $N^d_\uparrow(E_F) = 0$ (as in Ni) we get

$$R^{dip} = \frac{4\pi}{3}\hbar^3 k_B \gamma_e^2 \langle r^{-3}\rangle^2 \frac{3}{196}[N^d_\downarrow(E_F)]^2 f_\downarrow(2-f_\downarrow) \qquad \underline{N^d_\uparrow(E_F) = 0} \tag{33}$$

It is interesting to compare the dipolar relaxation rate with the orbital one. We consider again the case with $N^d_\uparrow(E_F) = 0$, for the sake of simplicity:

$$\frac{R^{dip}}{R^{orb}} = \frac{3}{196}\frac{(2-f_\downarrow)}{(2-\frac{5}{3}f_\downarrow)} \qquad \underline{N^d_\uparrow(E_F) = 0} \tag{34}$$

The ratio does not change very much with $f_\downarrow$. For instance, with $f_\downarrow = 0.6$ (spherical symmetry of the 3-d wavefunction) we have

$$\frac{R^{dip}}{R^{orb}} = 0.0214 \quad \text{(with } f_\downarrow = 0.6 \text{ and } N^d_\uparrow(E_F) = 0\text{)}$$

so that the dipolar relaxation rate is about 2% of the orbital rate.

E. Other Mechanisms

Core s-electrons are polarized by s-d exchange, if the d sub-bands are split, as in ferromagnetic metals. This polarization is sensed by the nucleus through contact interaction, and it is one of the important mechanisms of the hyperfine field. Therefore, there is an interaction between the nuclei and the d-electrons through polarized core s-electrons. The appropriate Hamiltonian involves terms of the form I_+S_- and I_-S_+. Following the same steps of the previous cases, we would have relaxation processes where the nuclear spin flips and the d-electron spin flips in

the opposite direction. Such processes would not be possible in nickel metal because the density of states at the Fermi surface of spin up electrons is almost zero.

Another mechanism of relaxation would be production of magnons. Only direct processes must be considered, since it is always observed that the relaxation rate is proportional to the temperature. Conservation of energy requires that the emitted or absorbed magnon has the same energy as the nuclear transition. Let us estimate if this is possible in a real situation. The magnon dispersion relation[28] has a constant term proportional to the anisotropy field H_A:

$$\hbar\omega(k) = g\mu_B H_A + 2JSa^2k^2$$

This formula is valid for cubic symmetry, with lattice constant a. J is the exchange integral and S the electronic spin.

From here we can calculate the minimum associated frequency f_{min} of the magnon spectrum:

$$f_{min} = \frac{g\mu_B}{2\pi\hbar} H_A = \frac{g\mu_B}{2\pi\hbar} \times \frac{2K}{M_S}$$

where K is the anisotropy constant and M_S is the saturation magnetization.

Substituting $K = 5 \times 10^4$ erg/cm^3, $M_S = 500$ gauss and $g = 2.21$, we get

$$f_{min} = \frac{2.21 \times 0.927 \times 10^{-20} \times 2 \times 5 \times 10^4}{6.626 \times 10^{-27} \times 500}$$

$$= 650 \text{ MHz}.$$

But the Larmor frequency in Ni metal is of the order of 30 MHz only. We do not expect, therefore, that relaxation through magnons will have any contribution to the total relaxation.

Thus for nickel metal we are left with the main mechanisms: contact relaxation Eq. (25), orbital relaxation Eq. (31), and dipolar relaxation Eq. (34). Numerical calculations are performed in Chapter IV, showing that the orbital relaxation is dominant and the others are a small percentage of the first.

III. EXPERIMENT

This chapter presents a detailed account of the experiment done. Part A describes the apparatus used. Part B tells how the samples were prepared. Finally, Part C gives the results and a preliminary evaluation.

A. Apparatus

A block diagram can be seen in Fig. 2. The transmitter provides the necessary rf pulses for saturating the nuclear Zeeman levels and for monitoring the recovery to the equilibrium nuclear magnetization. The transmitter is a pulsed oscillator, Arenberg type PG-650. It generates rf bursts when positive pulses, about 20 V, are applied to its input. With a 50 Ω load, the rf voltage may be as high as 600 V peak to peak, which means about 450 W instantaneous power.

The receiver (Fig. 3) consists of an rf amplifier and a detector. The rf amplifier is a cascade of amplifiers designed to provide several volts to feed into the detector.

Our configuration is not common. Usually, the rf level is smaller and the output of the detector goes into a low frequency amplifier (video or audio amplifier). The response of such a system is not linear because of the well-known knee of the diode I-V characteristic (occurring at about 0.3 V for germanium diodes). For signals smaller than the knee voltage, the detector follows approximately a square law. There are three ways to overcome this difficulty:

1. Use of a more elaborate detector circuit, such as an operational amplifier with the diode in the feedback loop.[29] In our case, it was not possible because there was not available an operational amplifier that would work at such a high frequency as 30 MHz.

2. Use of a phase detector circuit,[30] which is inherently linear. This configuration requires that the signal must be coherent in phase with the C. W. oscillator. The pulsed oscillator must be substituted by a pulsed amplifier driven by the same C. W. oscillator. We found that such changes were not simple to perform in the Arenberg oscillator (that was already available), so that this alternative was abandoned.

3. Calibration of the system response and reduction of the data. This is the scheme we adopted. Since we were using a digital computer to calculate the relaxation time, it was easy to add a subroutine to the main program to calculate a correction. However, we considered it necessary to linearize the detector response as much as possible in order to avoid errors introduced in the averaging process. To show it more clearly, let us suppose that the system has a square-law response. Then if x is the input, the output of the receiver is x^2 (neglecting the gain). The averager gives $\langle x^2 \rangle$, and the computer subroutine used to correct for the lack of linearity gives $\sqrt{\langle x^2 \rangle}$. This output may have an important error, especially for low signal-to-noise ratios, since $\sqrt{\langle x^2 \rangle} \neq \langle x \rangle$. That is the reason why we tried to linearize the detector responses by connecting a high gain rf strip, whose output was typically 5 V. A video amplifier was not necessary. On the contrary, we had to attenuate the detector output in order to avoid saturation of the averager.

The attenuator (connected between the preamplifier and the first wide band amplifier) is used as an overall gain control.

The sample was placed inside a coil L (Fig. 2). The capacitor C is tuned to series resonance at the transmitter frequency. When properly

tuned, the series LC circuit looks like a resistive load at the end of the transmission line. This resistive load is determined mainly by the sample losses. We measured for the coil a Q value of 10 to 15, which is small in comparison with the Q measured without the sample inside the coil (60 to 100).

The capacitor C must be very close to the coil L to get the maximum power transfer to the sample. It was found convenient to substitute the variable capacitor C by an adjustable transmission line with a short-circuited end (Fig. 4). The advantage of this device is that it is very easy to tune in any circumstance over a wide range. This was not the case with the discrete capacitor, which was difficult to manipulate when cooled down to helium temperatures.

The same coil L is used to pick up the nuclear signal. It is connected to the receiver through another transmission line. In order to uncouple the transmitter to the receiver the following measures were taken:

1) a pair of 1N3728 diodes were connected back-to-back and inserted in series at the transmitter output. Another pair of diodes was connected in parallel with the input to the receiver. These diodes have a different behavior when transmitter pulses or the signal appear in the circuit. The knee in the I-V characteristics makes them of a low impedance for strong signals and high impedance for small signals. The threshold occurs at about 0.5 V. The diodes at the transmitter output do not present a series impedance for the strong rf transmitter pulses. However, they effectively prevent the weak nuclear signal from being dissipated partly at the transmitter coil.

2) The transmission line going to the receiver has a $\lambda/4$ length. The result is that for strong signals the diodes across the receiver input protect the receiver by short-circuiting its input. However, looking from the transmitter, the receiver appears as an open circuit.

The rf power transferred to the sample coil is maximized when the series L-C circuit presents a resistive impedance equal to the characteristic impedance of the transmission line, 50 Ω in our case. We obtained the best match by trail and error with the help of a standing wave ratio indicator and an a.m. signal generator (H.P. model 608-B). The receiver was disconnected for this operation (Fig. 5). The standing wave ratio indicator measured both the incident and the reflected wave. It was built according to the specifications of the Radio Amateur's Handbook.[31]

Actually the effective impedance of the load is not very critical for matching purposes. If ρ is the reflection coefficient at the load, we have that the power P dissipated by the load is:

$$P = P_m(1 - |\rho|^2)$$

where P_m is the maximum power when the load equals the characteristic impedance of the line. For instance, if $\rho = 30\%$, then $P/P_m = 91\%$, which is quite good.

For a frequency of 30 MHz it was found that a 14 turn coil of 1 cm diameter was satisfactory. The same coil was used for the Ni^{61} resonance at 27 MHz and the Pd^{105} resonance at 33 MHz, with a power transfer better than 95% in both cases.

The same configuration of Fig. 5 was used at the beginning of each experiment for tuning.

The averager in Fig. 2 is a device that stores the results of many measurements and gives their average. It was necessary in our experiment because the nuclear signals were usually weak, of the same order of magnitude as the noise produced in the first stage of the preamplifier (about 2 μV rms). Besides, the saturation measurements of the spin-lattice relaxation time requires a good accuracy of the measurements, since one is interested in the difference between the equilibrium magnetization and the transient magnetization. When this difference is small (for long times, of the order of T_1 or more) its relative error may be much bigger than the relative error of the measurements.

Three configurations of the experimental setup were used, as described later. In the first two, the averager was a boxcar integrator (Fig. 6), which stores the measured voltage in a capacitor. It is essentially a low-pass filter that averages out the noise, while giving a dc output equal to the signal. The electronic switch is on only when the signal appears (for 1 to 2 μsec). In the last configuration (Fig. 7) the averager converted the analogic signal into digital form and stored it in an electronic computer, so that each new measurement would add up to the previous measurements (as described by Samuelson and Ailion).[32]

The control unit in Fig. 2 provides conveniently-timed pulses to operate the transmitter and the gate of the averager. The control pulses are the following: first a series of pulses which produce the rf "comb" used to excite the nuclear spins. Next, two pulses that produce two rf bursts for the spin echo. Finally, a pulse to trigger the boxcar when the signal is going to appear. The sequence in shown in Fig. 8.

We built three different configurations that were successive

improvements to cope with the noise problem.

In the first configuration, an initial comb of pulses was produced by a combination of Tektronix pulse generators type 162 and 163. The delay t_α (Fig. 8) was produced by a pulse generator built in the electronic shop of the Physics Department and adjusted manually. The last echo pulses were produced by a digital timer, controlled by a 1 MHz crystal oscillator. The same device gave the pulse for the boxcar. Actually the boxcar consisted of two identical units whose outputs were subtracted in an operational amplifier. The gates for the boxcars were displaced in time; one of them occurred when the signal appeared and the other was off the signal. This disposition eliminated any displacement of the signal baseline. Both the digital timer and the boxcars were built in the Electronics Shop.

The system worked well and gave acceptable results when the signal-to-noise ratio was high and the relaxation time was short. For lower signal-to-noise ratios, such as those in our experiments, it was necessary to increase the time constant of the boxcars. Then a new difficulty appeared: a slow drift of the system gain was noticeable for times of the order of one hour. The experiment consisted of measuring the signal for several values of t_α (typically 15). Each measurement was repeated for half an hour or more, so that by the end of the experiment the drift spoiled the initial accuracy of each average.

We eliminated this difficulty in the second configuration. Here, we measured a reference signal together with the desired signal. Both measurements were made alternatively and averaged in two independent boxcars. For the reference signal, the value of t_α was always the same

and several times higher than the expected T_1. Several pulse generators and logic gates provided the automatic alternation of both measurements.

The third configuration also eliminated the drift problem and reduced the total duration of the experiment to one half. It consisted basically in changing the value of t_α automatically for each new measurement, and storing the result in a separate channel of a multichannel analyzer. After the complete series of pre-set values of t_α had passed, the system started again, adding the new results to the previous ones. The reference signal is not needed in the third configuration, since the slow drifts are shared evenly by all the averaged results. That is why the experiment time is reduced to one-half in comparison with the second configuration.

The multichannel analyzer we used was a TMC Model 404, working in the multiscalar mode. The voltage to frequency converter was a Vidar Model 240. It was connected to the multichannel analyzer via a gated decade counter, that reduced the frequency by a factor of 1/10. More counters and logic gates provided the automatic change of t_α and controlled the address advance of the multichannel analyzer. The "sample and hold" device was the same boxcar used before, but the time constant of the RC circuit was set to 0.2 μsec, which was smaller than the opening of the gate (1 to 2 μsec).

B. Sample Preparation

Samples of non-annealed nickel were simply obtained from Ni sponge of 99.999% purity, supplied by Johnson-Matthey. The metal powder was mixed with N-grease for electrical insulation, thus avoiding the effect of skin depth. The N-grease also improved the thermal contact between

the metal particles and the helium bath.

The experiment with annealed nickel was made with the same Ni sponge after a heat treatment at 600°C for two hours. It was performed in an Abar resistance furnace with high vacuum facilities. The residual pressure was kept under 4×10^{-6} torr. Alumina powder was added to avoid sintering of the nickel particles.

The Ni-Pd was prepared by melting Ni and Pd sponge in an alumina crucible in the same Abar furnace. There was a reducing atmosphere of hydrogen at the beginning to eliminate surface oxidation and facilitate the process. Actually the gas was a mixture of 4% H_2 and 96% He. Later, the gas was substituted by pure He. In this way we prevented H_2 from being disolved in the liquid melt and released upon solidification, thereby producing bubbles.

The alloy was kept at 20°C below the melting point for 24 hours in order to homogenize it. Later, the degree of homogeneity was tested with an electron beam microprobe at IMRD. The instrument could detect variations of composition of the order of 1% or larger. It was found in our sample that the local fluctuations of composition were below the limit of sensitivity of the instrument.

The alloy was ground against a rotating disc covered with abrasive alumina paper #120. Later, the alloy particles were easily separated from the alumina particles with the help of a magnet.

The last step was annealing for two hours at 600°C in a high vacuum to eliminate the strains produced by the cold work.

The samples for the experiments consisted of a mixture of metal particles and N-grease. The latter provided electrical insulation between the particles, to avoid the effect of skin depth.

C. Results

1. Observation of NMR in Ni^{61} and Pd^{105}.

The spin echo technique was used. The sample temperature was 4.2°K. Without an external magnetic field we got a resonance frequency of 28.46 MHz for Ni^{61}, both in pure Ni and in the Ni-Pd alloy, in agreement with earlier measurements[33] that used a marginal oscillator as a c.w. detector of NMR.

We reproduced the results of Aubrun and Khoi[34] and Bancroft[20] when an external magnetic field was applied. The resonance frequency shifted down, and for external fields higher than about 4.5 kG, the variation was linear. This shows that the hyperfine field at the Ni^{61} nucleus is negative and that the particles become magnetically saturated for external fields higher than 4.5 kG.

This argument is reinforced by the fact that the intensity of the echo went down as the magnetic field was increased. This shows that the domain walls disappeared, because the enhancement factor[35] was much bigger in the walls than in the bulk domain.

We obtained additional evidence of the change of enhancement factors when going from the zero external field situation to that with an external applied field. We observed the shape of the echo as a function of the amplitude and width of the rf pulses. If the turning angles were very high (much bigger than $\pi/2$), the signal appeared as described by Mims.[36] For instance, if the two rf pulses had the same width, the echo was symmetrical, with a dip in the center. If the rf amplitude was reduced, so that the turning angle became of the order of $\pi/2$, the echo would have a maximum in the center (as commonly happens). This center

was displaced with respect to the previous case: It occurred at a time $t_1/2$ later, where t_1 was the rf pulse width.

These changes were not seen when an external magnetic field was applied. We observed only the last case (even with the highest possible rf field), showing that the turning angle was of the order of $\pi/2$ and that the enhancement factor was small.

Since the nuclei do not experience a demagnetizing field in the center of a wall, the value of the resonance frequency at zero applied field gives directly the hyperfine field. In the case of Ni^{61}, it turns out to be -75 kOe, as calculated by Streever and Bennett[33] and using the ENDOR measurement of the Ni^{61} nuclear magnetic moment.[37]

The Pd resonance in the Ni-Pd alloy was found at 33.79 MHz (without an external magnetic field). This result agrees with the calculated hyperfine field of 194 kOe reported by Kontani and Itoh,[38] also obtained in a spin echo experiment at 4.2°K. We found that the sign of the hyperfine field is negative, as in Ni, because the resonance frequency shifted down when an external magnetic field was applied. Figure 9 shows the results for Pd resonance together with Bancroft's measurements in Ni sponge.[20] The frequency scales are different for each display; they are of different size and different origin. They are determined by the condition that the straight line for Ni resonance coincides with the one for Pd. These straight lines represent the theoretical resonance frequency vs external field of single-domain spherical particles having a demagnetizing field of 2.3 kG (as calculated by Bancroft). For external fields higher than about 4 kG, the experimental points coincide with the straight line, showing that the Ni particles are indeed single domains,

so that there are no walls present. Our measurements of Pd resonance did not pretend to prove this fact, which was already established, so that we did not spend too much time trying to improve the accuracy to get closer to Bancroft's curve. Qualitative agreement is satisfactory enough.

In the course of these measurements, care was taken to set the turning angle to a value small enough, so that the echo frequency would be the same as that of the exciting rf pulses. This would not be the case for high turning angles, giving wrong values of the resonant frequency (as reported by Budnick and Skalski[40]).

It was found that after repeating the experiment several times, the signal decreased until it was completely buried in noise. This effect has not been reported before. We believe it was caused by an increase of the line width beyond the receiver bandwidth (about 1 MHz). This could be produced by a slight oxidation of the sample, with lattice distortions that would broaden the NMR line through electric quadrupole effects (note that Ni^{61} has a 3/2 nuclear spin and Pd^{105} has a 5/2 nuclear spin; the electric quadrupole moments are[39] 0.134 barns for Ni^{61} and 0.8 barns for Pd^{105}). The oxidation process might be enhanced by the repetition of the thermal cycle (between room temperature and liquid helium temperature) through an increase in the number of dislocations of the sample. Hammond and Knight[41] made an experiment of nuclear quadrupole resonance in superconducting gallium particles suspended in oil or paraffin wax. They found a broadening of the resonance line and a severe loss in intensity in comparison with the same experiment performed in gallium particles mixed with quartz

particles of comparable size. They attributed it to strains produced by the contraction of the frozen oil or wax at low temperatures. The same effect in our N-grease might well be part of the cause of the deterioration of the signal.

2. Measurement of Relaxation Times.

The recovery of the magnetization, as measured by the spin echo signal, was exponential after some time had passed. At the beginning, the relaxation was faster. This is explained in terms of diffusion of the nuclear excitation from nuclei in the center of the NMR line to nuclei at the sides, when the latter were not excited by the rf comb.[20] There are also nuclei at the center of the NMR line that are not excited because of being too far from the surface of the sample (at a distance bigger than the rf penetration depth). We observed this effect in our experiments in the following way. We assumed a theoretical relaxation function with an additional adjustable parameter that took into account the diffusion and we adjusted the parameters in a least-squares fit to the experimental data. The relaxation function is:

$$M(t) = M_o\{1-\exp[-(t+t_o)/T_1]\}$$

where M(t) is the time-dependent z-nuclear magnetization, M_o its static value, T_1 is the spin-lattice relaxation time and t_o takes into account the fact that the magnetization relaxes faster at the beginning, up to a time t' (of the order of the spin-spin relaxation time T_2, according to Portis[42]) and after that it follows the exponential (Fig. 10). This is equivalent to displace the t-axis in t_o for the subsequent relaxation. Upon the substitution $\beta=\exp(-t_o/T_1)$ we get:

$$M(t) = M_o[1-\beta \exp(-t/T_1)].$$

In this equation, M_o, β, and T_1 are unknown parameters to be calculated in a least-squares fit to the experimental data of (M,t) pairs. The computer program is described in the appendix.

The results always gave $\beta<1$, showing that there is indeed some diffusion of the spin excitation. A typical value is $\beta = 0.85$. It depended on the amplitude of the rf comb, the number of pulses, their separation and width. The best results were obtained with a comb of 10 to 20 pulses, at the maximum transmitter voltage. The pulse separation was 1 to 2 msec (note that T_2 is of the order of 10 msec[43]), and the pulse width, about 10 μsec. The two rf pulses used to generate the echo had a width of 2 μsec and a separation of 500 μsec. This somewhat long time was necessary for the recovery of one of the wide band amplifiers (Hewlett-Packard model 462-A) after being saturated by the rf pulses. However, it is still much smaller than T_2, so that the echo is not reduced. A typical relaxation curve can be seen in Fig. 11. The experiment was run under the above conditions. In Fig. 11, $[1-M(t)/M_o]$ is plotted as a function of time in a semi-logarithmic graph. The sample was pure Ni, annealed.

We expected to get a better saturation by increasing the comb length. However, we found much larger relaxation times and a non-exponential relaxation (Fig. 12, curve a)). The relaxation time increased with the length of the comb. We got relaxation times more than 10 times bigger than those obtained with short combs (of about 10 to 20 pulses). In Fig. 12, curve a), the comb had 800 pulses, separated 2 msec. For comparison, curve c) is a repetition of Fig. 11, but at the same time

scale of curve a). The explanation of this strange effect is simple: with long combs, the temperature of the whole sample increased, by eddy-currents and magnetic losses. We noted also that the liquid helium bath boiled at a much higher rate. For an additional proof, we made the following experiment: the transmitter frequency was shifted by 4 MHz (more than the linewidth), and a long comb at the new frequency was applied. The z-nuclear magnetization was monitored with another transmitter, in the usual way (two pulse echo), working at the Larmor frequency. We could see a similar relaxation curve, in spite of the fact that the nuclear spins were not excited by the comb. This showed that the whole sample was heated and that we were monitoring the sample-bath thermal relaxation!

We observed also a non-exponential relaxation curve in non-annealed pure Ni samples (Fig. 12, curve b)). The shape suggests broadening through strain-induced quadrupolar interactions, as found by Andrew and Turnstall,[44] Simmons, Sullivan and Robinson[45] and Narath.[46] The rf comb was not strong enough to saturate all the Zeeman levels: only the central transition was excited. After annealing the sample, we obtained a purely exponential curve like c). It is not obvious why curve c) has a faster relaxation time than curve b); we believe that in the latter, there was an additional effect, probably surface oxidation, closely connected with the deterioration of the signal that was explained before. Besides, it was found that after repeating the experiment with the alloys, the relaxation times tended to increase. However, the pure Ni samples were much more stable. Note that in the latter, the particles had a roughly spherical shape, while in the alloys the particles were rod-like

(with a bigger surface area). This fact reinforces the oxidation hypothesis.

The accuracy of our results is not determined by the errors of our measurements, but by the change in sample properties. For pure Ni samples, we obtained relaxation times from 47 to 52 msec when the temperature was 4.2°K and the external magnetic field 6 kG. As a final value we shall use in the next chapter: T_1 = 50 msec ± 5%.

In the Ni-Pd alloy, 2 at.% concentration, the Ni^{61} relaxation time varied from 43 to 61 msec in the same conditions of temperature and magnetic field. Note that the average is about the same of the pure Ni.

The Pd relaxation time is not needed in absolute value in the next chapter. We are interested only in the ratio R_{Pd}/R_{Ni}. Fortunately, when we measured the Pd relaxation, the Ni relaxation in the alloy was rendering about 50 msec so that the Pd value can be well considered the average. We got T_1 = 580 msec for Pd^{105} at 4.2°K.

We tested the constancy of the product T_1T for the Ni^{61} relaxation in the alloy. We made two consecutive measurements at 4.2°K and 2.1°K (in order to avoid the oxidation drift). We obtained T_1 = 61 msec at 4.2°K and T_1 = 128 msec at 2.1°K, so that T_1T is constant within the experimental error.

IV. INTERPRETATION OF RESULTS

This chapter is a critical study of the experimental results of the third chapter. In Part A, we calculate the relaxation rate of Ni using the theoretical formulas derived in the second chapter. Good agreement with the experimental values strongly supports the orbital relaxation model. This model is used again in Part B to obtain a Pd 4-d density of states from the experimental relaxation rate of Pd in Ni. The new result helps to develop a model of the Pd impurity state in Ni in Part C. Then it is compared with other experimental facts in Part D.

A. Nickel Relaxation

Here we compare the experimental result of Ni relaxation time with theoretical calculations employing the formulas derived in the second chapter.

Starting with the orbital relaxation (we shall see that it is dominant) we need numerical values for $\langle r^{-3} \rangle$, $N_\sigma(E_F)$ and f_σ.

We obtained the average $\langle r^{-3} \rangle$ from a table of atomic wave-functions (calculated by Herman and Skillman[47]) and a numerical integration according to Simpson's rule. The computer program is shown in the appendix. The result is:

$$\langle r^{-3} \rangle_{Ni} = 7.86 \text{ a.u.} = 5.31 \times 10^{25} \text{cm}^{-3}$$

We assume that $\langle r^{-3} \rangle$ in the metal is the same as in the free atom. It seems reasonable, since the 3-d electrons are quite localized in the metal.

The density of states at the Fermi surface, $N^d(E_F)$ is taken from an APW band structure calculation for Ni metal.[48] We assume that

$$N^{d}_{\uparrow}(E_F)+N^{d}_{\downarrow}(E_F)+N^{s}(E_F) = N(E_F) = 1.7\times10^{12} \text{ el (erg atom)}^{-1}$$

and $N^{d}_{\uparrow}(E_F) = 0$.

$N^{s}(E_F)$ is a small correction. It can be calculated from a free electron model. In this model, the density of states per atom is given by:

$$N(E) = \frac{V_o}{2\pi^2}\left(\frac{2m}{\hbar^2}\right)^{3/2} E^{1/2}$$

where V_o is the atomic volume. Defining n as the number of electrons per atom, we get the Fermi energy from:

$$E_F = \frac{\hbar^2}{2m}\left(\frac{3\pi^2 n}{V_o}\right)^{2/3}$$

Hence:

$$N(E_F) = \frac{m}{\pi^2\hbar^2}(3\pi^2 V_o^2 n)^{1/3}$$

The next element to nickel in the periodic table is copper, with a similar structure but only s-states at the Fermi energy. Its density of states is known from an APW band structure calculation by Burdick.[49] Now,

$$\frac{N^{s}_{Ni}(E_F)}{N^{s}_{Cu}(E_F)} = \frac{(V_o^2 n)^{1/3}_{Ni}}{(V_o^2 n)^{1/3}_{Cu}}$$

The s-electron densities are: for Cu, one electron per atom and for Ni, 0.6 electron per atom. The ratio of the atomic volumes is obtained from the lattice constants: 3.61 Å for Cu and 3.52 Å for Ni. Hence:

$$\frac{N^s_{Ni}(E_F)}{N^s_{Cu}(E_F)} = (\frac{3.52}{3.61})^2 \times (0.6)^{1/3} = 0.8.$$

From Burdick,

$$N^s_{Cu}(E_F) = 3 \text{ el(Ry atom)}^{-1} = 1.4\times10^{11} \text{ el(erg. atom)}^{-1}.$$

Hence, $N^s_{Ni}(E_F) = 1.12\times10^{11}$ el (erg. at.)$^{-1}$. It is about 7% of the total denisty of states.

Hence:

$$N^d_{\downarrow}(E_F) = 1.59\times10^{12} \text{ el(erg. atom)}^{-1}$$

The last parameter needed is f_σ. Mook[50] made measurements of Bragg diffraction of polarized neutrons in Ni metal and found that $f_\downarrow = 0.81$.

Replacing all the parameters in equation (31) and (34) of chapter two, we get:

$$R^{orb}_{Ni} = 0.79\times10^{-6}$$

$$R^{dip}_{Ni} = 0.028\times R^{orb}_{Ni}$$

$$= 0.022\times10^{-6}.$$

Finally, we estimate the s-contact relaxation indirectly, from relaxation data of copper metal. Assuming that in the latter the s-contact relaxation is dominant, we have

$$\frac{R^s_{Ni}}{R^s_{Cu}} = \left[\frac{N^s_{Ni}(E_F)}{N^s_{Cu}(E_F)}\right]^2 = 0.8^2 = 0.64$$

Relaxation time in Cu metal was measured by Anderson and Redfield.[51] They found $T_1T = 1.27$ for Cu, hence:

$$R^s_{Cu} = 0.016\times10^{-6}$$

$$R^s_{Ni} = 0.0102\times10^{-6}.$$

Thus the s-contact relaxation in Ni is 1.3% of the orbital relaxation. Adding the three effects we get:

$$R_{Ni} = R^{orb}_{Ni} + R^{dip}_{Ni} + R^s_{Ni} = 0.82\times10^{-6}.$$

Moriya[24] made a similar calculation with less accurate parameters. He used an average $\langle r^{-3}\rangle$ obtained from atomic hyperfine data (that was smaller than our calculation from Herman and Skillman's wavefunctions) and a density of states derived from specific heat measurements. We preferred to use a density of states obtained from a band structure calculation, which gave a smaller value. This is expected because the specific heat in enhanced by the electron-phonon interaction and the electron-magnon interaction.[52] However, both errors in Moriya's paper went in the opposite direction and almost compensated. After correcting a numerical error of 4 in his density of states, we find that his result is almost equal to ours.

The experiment reported in the last chapter gave $T_1 = 0.05$ sec for Ni at $T = 4.2°K$. From this experimental data we get:

$$(\gamma_n^2 T_1 T)^{-1} = (2380^2\times0.05\times4.2)^{-1} = 0.84\times10^{-6} \text{ (exp)}.$$

We can see that theory and experiment agree within 2.5%. We believe the main reason for this good agreement is that the interpretation

of the experiment was closer to the real situation. The external magnetic field effectively swept away the domain walls, so that the only relaxation mechanisms were precisely those considered here. At the time of Moriya's paper publication, the results of the measurements were affected by domain wall relaxation. This mechanism is very powerful and was not considered in the interpretation.

B. Palladium Relaxation

Since the orbital interaction was well established as the dominant mechanism of relaxation, we can use the experimental value of the relaxation time to obtain the 4-d density of states at the Fermi level of the Pd impurity. From formula (31) we get:

$$\frac{R_{Pd}^{orb}}{R_{Ni}^{orb}} = \left[\frac{\langle r^{-3}\rangle_{Pd}}{\langle r^{-3}\rangle_{Ni}}\right]^2 \frac{\left\{[N_{\downarrow Pd}^{4d}(E_F)]^2 + [N_{\uparrow Pd}^{4d}(E_F)]^2\right\}}{[N_{\downarrow Ni}^{3d}(E_F)]^2}$$

Hence,

$$\sqrt{[N_{\downarrow Pd}^{4d}(E_F)]^2 + [N_{\uparrow Pd}^{4d}(E_F)]^2} = \frac{\langle r^{-3}\rangle_{Ni}}{\langle r^{-3}\rangle_{Pd}} N_{\downarrow Ni}^{3d}(E_F) \sqrt{\frac{R_{Pd}^{orb}}{R_{Ni}^{orb}}}$$

Here we assumed that the f coefficients for the Pd impurity are equal to those of Ni. This assumption can be removed without too much change in the final results, since the relaxation rate does not depend very strongly on f.

The average $\langle r^{-3}\rangle$ for 4-d orbitals in Pd is calculated in the same way as the one for 3-d orbitals in Ni. We get:

$$\langle r^{-3}\rangle_{Pd} = 7.65 \text{ au} = 5.16\times10^{25} \text{ cm}^{-3}.$$

From the experimental result of the third chapter, $T_1 = 0.58$ sec at 4.2°K for Pd, we get:

$$R_{Pd}^{orb} = 0.34\times10^{-6} \text{ (exp)}.$$

Hence,

$$\sqrt{[N_{\downarrow Pd}^{4d}(E_F)]^2 + [N_{\uparrow Pd}^{4d}(E_F)]^2} = \frac{5.31}{5.16}\times1.68\times10^{12}\sqrt{\frac{0.34}{0.84}}$$

$$= 1.1\times10^{12} \text{ el(erg atom)}^{-1}$$

C. Description of the Impurity State

The problem of finding the impurity levels has not yet been solved quantitatively. In the Ni-Pd case, all we can do is to gather several experimental facts (including our measurements) and propose a structure that would agree reasonably well with all of them.

Friedel[12] gave a phenomenological description of the impurity problem, especially useful to explain the appearance of localized moments at the impurity in non-magnetic hosts. Later, his concepts were extended and treated more quantitatively by Anderson[13] for impurities that develop a magnetic moment and by Wolff[14] for non-magnetic impurities.

According to Friedel, the impurity gives away its outer shell of electrons to the conduction band of the host; a strong attractive potential appears at the impurity site. This potential attracts conduction electrons, which screen it within a short distance. The strength of the potential determines whether or not the screening electrons are actually bound to the impurity. If the electrons are not bound, the electronic charge density in the vicinity of the impurity

is very high because of resonances of the scattering cross sections at electron energies near those of the vacated levels. This is called a virtual bound state. It behaves similarly to a bound state, but the fact that it is close to the Fermi energy gives rise to special effects.

Let us study all the possibilities for the 4-d states of the Pd impurity in Ni (Fig. 13). The spin up and spin down states are drawn separately to take into account a possible splitting. In all cases, the ordinates represent the electron energy with respect to the Fermi energy and the abscissae are the impurity density of states. The area under each sub-band corresponds to five electrons per atom. States are filled up to the Fermi energy (shadowed areas).

Several considerations will allow us to select one of the cases as the one that appears in the Ni-Pd alloy.

The first one is neutrality of the impurity. It is known that any localized potential is screened by conduction electrons within a very short length, smaller than the interatomic distance. Because of the similarities of the core potential of Ni and Pd (same valence), we can be sure that screening electrons for Pd go to 4d and 5s states. This situation excludes immediately cases f, g, h and i in Fig. 13 because no more than two 5s states are allowed, so that there should not be more than two holes in the 4d band. Cases g and i would have ten holes and for cases f and h, the number of holes would be between five and ten.

Next consideration is the splitting of the impurity levels because of the ferromagnetic state of the Ni host. It is easy to understand it in terms of a molecular field. Since there are exchange interactions between the 3d band of Ni and the 4d impurity levels, we may assume

there is a molecular field acting on the latter. Its value must be of the same order of magnitude of the molecular field assigned to the 3d band of Ni. We can neglect cases a, d and g because the levels are not split there.

The results of our measurements of the spin-lattice relaxation time tell that there is a sizeable density of states of the impurity level at the Fermi energy. Because of this experimental fact, we eliminate case c.

The only remaining possibilities are b and e.

Note that case b is similar to the 3-d band in nickel metal. We are going to study this case some more and get some consequences that can be compared with other experiments.

It is interesting to estimate the number of holes in the $4d\downarrow$ levels. Let us assume that the density of states vs energy curve has a parabolic shape near the Fermi energy, or $E \sim [N(E)]^2$ where E is the energy measured from the intercept of the curve with the E axis, so that $N(0) = 0$. The number of holes n_h is given by:

$$n_h = \int_o^{E_F} N(E)dE \sim E_F^{3/2}$$

$$n_h \sim [N(E_F)]^3.$$

We obtain a rough estimate of n_h by assuming that the Ni 3d band has the same shape and using the known values of $N(E_F)$ and n_h for Ni. The latter comes from measurements of the saturation magnetization[66] and the g-factor[55]

$$\frac{(n_h)_{Pd}}{(n_h)_{Ni}} = \frac{[N_{Pd}(E_F)]^3}{(N_{Ni}(E_F)]^3}$$

$$N_{Ni}(E_F) = 1.7\times10^{12} \text{ states/erg atom}$$

From Part B we obtain:

$$N_{Pd}(E_F) = 1.1\times10^{12}$$

$$(n_h)_{Ni} = 0.565 \text{ holes/atom}$$

$$(n_h)_{Pd} = 0.565\times(\frac{1.1}{1.68})^3$$

$$= 0.16 \text{ holes/atom}$$

In order to examine the possibility of case e, let us estimate the splitting of the 4d sub-bands of the impurity. We may assume in a first approximation it is of the same order of the splitting of the 3d sub-bands of Ni. The latter is not known accurately. Connolly[48] found a 0.9 eV splitting in an APW calculation of the band structure. Zornberg[53] obtained a smaller splitting between 0.4 and 0.6 eV, from optical spectra data. Phillips[54] tabulates the results of many authors, ranging from 0.3 to 1.7 eV, and finally estimates a splitting of 0.5 ± 0.1 eV in coincidence with Zornberg.

A 0.5 eV splitting would eliminate immediately case e of Fig. 13 because the density of states at the Fermi surface would be higher than the Ni 3d density of states. Our measurements show just the opposite result: $N_{Pd}^{4d} < N_{Ni}^{3d}$.

On choosing model b, there are two important consequences: 1) a density of states that agrees with our measurements of spin-lattice relaxation time and 2) a small magnetic moment localized at the impurity. Its value is obtained from the calculated number of holes, $n_h = 0.16$ and the measured value of the orbital contribution. Fischer, Herr and

and Meyer[55] obtained for Pd a g-factor of 2.58 in Ni-Pd alloys. Hence:

$$\mu_{Pd} = \frac{2.58}{2} \times 0.16\ \mu_B = 0.21\ \mu_B.$$

We have to emphasize now that this result is the consequence of a simple model that assumes equal shape for the 4d impurity levels and the 3d Ni band.

D. DISCUSSION

Here we would like to compare the prediction of a moment of 0.21 μ_B localized at the Pd impurity (from our model) with the results of other experiments.

1. The Hyperfine Field at the Pd Nucleus

In ferromagnetic alloys the two dominant contributions to the hyperfine field are:[56] contact interaction by conduction electrons and contact interaction by s-core electrons. Both are polarized by s-d exchange. The core polarization is important if there is a localized moment at the impurity site. Shirley, Rosenblum and Matthias[11] calculated a conduction electron contribution of -79 kOe for the Pd impurity in Ni. Since the total hyperfine field is -194 kOe, there is an additional -115 kOe field that they attributed to s-core polarization. From that a magnetic moment of 0.3 μ_B at the Pd site was obtained.

Note that calculations of hyperfine fields use the exchange-polarized Hartree-Fock method,[56] where the wavefunctions of opposite spin direction are evaluated separately. The net spin density results as a difference between the two charge densities of opposite spins. The difference turns out to be much smaller than each term, so that there may be a large relative error. That is the reason why hyperfine

field calculations cannot be considered very reliable and their predictions of the Pd magnetic moment should not be taken more seriously than ours (based on the measurement of the density of states of the impurity).

2. Measurement of the Magnetic Moment by Neutron Scattering

Cable and Child[57] performed experiments of Bragg and diffuse scattering of polarized neutrons in four Ni-Pd alloys. The Pd concentration ranged from 25 to 92 at.%. The results are shown in Table II. Cable and Child adopted the diffuse scattering values as more accurately describing the situation. They predicted from them that the Pd moment would vanish for very dilute alloys (Ni-rich). Note that the experiment cannot be done for very dilute alloys because the method is not sensitive enough.

Cable and Child's conclusion on dilute alloys does not agree with ours at first sight. We have attempted therefore a more careful examination of their interpretation.

A very significant fact is that the Pd moments obtained from Bragg scattering are systematically bigger than those from diffuse scattering. The difference is larger than the estimated error in two cases. No explanation is given in the paper. We shall present here the arguments we draw against the diffuse scattering results.

In a polarized-neutron experiment, one measures the difference in cross sections, $\Delta\frac{d\sigma}{d\Omega}(K)$ for neutron spins parallel and anti-parallel to the magnetic moments of the alloy. It is given by the formula

$$\Delta \frac{d\sigma}{d\Omega}(K) = 4S(K)\ \Delta b \Delta p(K) \qquad (35)$$

where K is the scattering vector and S(K) is the scattering function given by

$$S(K) = c(1-c)\left[1 + \sum_{R} \alpha(R)\,\frac{\sin KR}{KR}\right]\ldots$$

Here, c is the Pd concentration, $\alpha(R)$'s are the short-range order parameters and R is a neighbor lattice vector. In formula (35), Δb is the difference between the Ni and Pd nuclear scattering lengths and Δp is proportional to the difference of magnetic scatterings:

$$\Delta p(K) = 0.27\times10^{-12}\left[\mu_{Ni}\, f_{Ni}(K) - \mu_{Pd}\, f_{Pd}(K)\right]$$

where f(K)'s are the form factors. Hence,

$$\Delta\,\frac{d\sigma}{d\Omega}(K) = 4c(1-c)\left[1 + \sum_{R} \alpha(R)\,\frac{\sin KR}{KR}\right]\Delta b\times0.27\times10^{-12}\left[\mu_{Ni}f_{Ni}(K)-\mu_{Pd}f_{Pd}(K)\right].$$

The short-range order parameters $\alpha(R)$'s and the magnetic moments were calculated in a least-squares fit to the experimental data of the cross-section difference as function of the scattering vector. Cable and Child found that it was sufficient to extend the summation in R to the first two neighbors, and that the calculated values of $\alpha(R)$'s were very small. So far, it was assumed that there were no local disturbances of the magnetic moment of any atom by the presence of a neighbor of the other type; in other words, all Ni atoms had equal moments and the same for the Pd atoms. If this requirement is dropped we get a factor of the same form of S(K),[58] so that it is not possible to distinguish between short-range order and neighbor magnetic disturbance or a combination of both effects. At any rate, Cable and Child recognized

that it was not possible to know accurately the $\alpha(R)$ parameters due to the small number of experimental data points and their huge statistical fluctuations. Consequently, they decided to neglect them and use $S(K) = c(1-c)$. Both difference cross sections (with and without the $\alpha(R)$ parameters) are plotted in Fig. 2 of Cable and Child's paper. After studying this drawing, we tend to disagree with the choice of $\alpha(R) = 0$ as being more meaningful. This choice is very important when calculating $(\mu_{Ni} - \mu_{Pd})$ from the extrapolation to K = 0 of the difference cross section:

$$\Delta \frac{d\sigma}{d\Omega}(0) = 4c(1-c)\,[1 + \alpha(R_1) + \alpha(R_2)]\,\Delta b \times 0.27 \times 10^{-12} \times (\mu_{Ni} - \mu_{Pd}).$$

Consider for instance the 25% Pd alloy. According to Fig. 2 of Cable and Child's paper, the extrapolations to K = 0 are:

$$\Delta \frac{d\sigma}{d\Omega}(0) = 66 \text{ mbarns (for } \alpha(R_1) = \alpha(R_2) = 0)$$

$$\Delta \frac{d\sigma}{d\Omega}(0) = 35 \text{ mbarns (for } \alpha(R_2) = -0.08).$$

Taking the first value we get $\Delta\mu = \mu_{Ni} - \mu_{Pd} = 0.74\ \mu_B$. Taking the second value we get $\Delta\mu = 0.39\ \mu_B$. In the first case, we get $\mu_{Pd} = 0$. In the second case, we get $\mu_{Pd} = 0.27\ \mu_B$.

We believe that the number of data points should be increased and the statistical fluctuations should be diminished before attempting to calculate a reliable value for the Pd moment in the 25% alloy. Besides, an extrapolation to dilute alloys should not be made unless many more alloys in the useful range are measured. So far, we think Cable and

Child's experiment does not disagree significantly with out conclusion, on account of their uncertainty in the zero-scattering vector extrapolation. A private communication with Dr. Cable, however, has failed to bring us to an agreement on this point.

3. Magnetization Curve of Ni-Pd Alloys

Crangle and Scott[59] and Fischer, Herr, and Meyer[55] measured the average magnetic moment per atom, M_{av}, as a function of concentration. They found that M_{av} decreases linearly with Pd concentration from 0 up to 50% Pd. In this region of concentration, the following relation is followed very closely:

$$M_{av} = (0.616 - 0.11\ c)\ \mu_B$$

where c is the Pd concentration. For $c > 0.5$, M_{av} drops faster and vanishes at about $c \approx 0.98$.

It was suggested that for $c < 0.5$, the Ni moment remains constant ($0.616\mu_B$) and each Pd atom contributes with $0.506\mu_B$. However, the Pd contribution does not need to be localized at the Pd atom. It can be shared by the neighbor Ni atoms, as proposed by Cable and Child.[58] Analogously, a positive or negative moment disturbance on the impurity neighbors has been found by neutron diffuse scattering in other alloys.[60-62]

Let us assume the Pd impurity has a $0.21\mu_B$ moment (as estimated here) and only the nearest neighbors have a bigger moment, so that the total Pd contribution is $0.506\mu_B$. Thus the twelve nearest neighbors have an extra moment of $(0.506 - 0.21)\mu_B = 0.296\mu_B$ and each one of them has an extra moment of $0.025\mu_B$, or a $0.64\mu_B$ total moment. Fig. 14 shows a cross section of the alloy lattice through a Pd atom, to illustrate the model.

We think the explanation of the enhanced Ni moment is part of the whole problem of the Pd states in Ni. Here we would like to mention a similar situation: Stearns[63] postulated that there is an anti-ferromagnetic indirect interaction via s-conduction electrons, to explain the Mössbauer spectra of alloys of iron with different impurities. If the same effect occurs in the Ni-Pd alloys, then the reduced moment on the Pd atom could well increase the moment on the Ni neighbors.

V. SUMMARY AND CONCLUSIONS

We detected the NMR and measured the spin-lattice relaxation time of Ni^{61} and Pd^{105} in a Ni-Pd alloy, 2 at.% concentration. The Ni^{61} relaxation time agrees with a theoretical model in which the dominant mechanism of relaxation is an interaction with orbital fluctuations of d electrons. Assuming that the same mechanism applies to the Pd^{105} relaxation, we derived the value for the density of states at the Fermi surface of the 4-d Pd levels. From there we inferred there is a magnetic moment at the Pd impurity, and estimated its value to be $0.21\mu_B$. The accuracy of this result is limited by the assumption that the 4-d Pd levels have a density of states curve of the same shape as that of the 3-d Ni levels. We adopted this assumption for lack of better data. This result does not disagree with experiments of diffuse neutron scattering and measurements of the hyperfine field.

Next, we proposed a model of magnetic moment distribution around the impurity, made to agree with bulk magnetization measurements. This model has only nearest neighbors perturbed with respect to the pure host. In order to test this model, it would be interesting to get the structure of the Ni^{61} NMR spectrum in the alloy. One would expect a satellite line, due to the different environment of the Ni^{61} nearest neighbors to the Pd impurity. A similar situation was found in a Co-Ni alloy by LaForce, Ravitz, and Day,[64] and Riedi and Scurlock.[65] We can estimate the displacement of the satellite line from the calculations of hyperfine fields by Shirley, Rosenblum, and Matthias.[11] Suppose there is only a change of the core polarization field produced by the change of the magnetic moment. In Ni metal, the calculated core

polarization field is -50 kG. Hence, in the nearest neighbors to the Pd impurity, we would have a change in the hyperfine field H_{hfs}:

$$\Delta H_{hfs} = -50 \times 0.028/0.616 = -2.28 \text{ kG.}$$

That means an increase of frequency of 0.86 MHz, which can be easily detected.

Our work is part of a wide-range project of study of different impurities in Ni. The first case was a Ni-Cu alloy, studied by Bancroft,[20] who found that there was no magnetic moment at the Cu site. The Cu impurity has very similar electron levels to Ni and differs only in one unit of valence. In our case, Pd has the same valence as Ni, but differs only in atomic size. We can see that Cu and Pd are two extreme cases, and that other impurities in Ni would have similar behaviors, approaching one of the two cases something intermediate. In particular, we are planning to work in first place with the following alloys: Ni-Pt, Ni-Ir, and Ni-Rh.

ACKNOWLEDGMENTS

I would like to thank Professor Alan M. Portis for suggesting the subject of this research work and for his invaluable help during its completion and during the writing of this dissertation. I am indebted to Professor Leo M. Falicov for very illuminating discussions that led to the interpretation of the experimental results. I acknowledge the advice of Dr. Michael H. Bancroft in guiding my first steps in the field of nuclear magnetic relaxation.

I have constantly benefited from the technical support of the Electronic Shop staff, especially Alexander George in design and Walter Fitelson and Peter Miller in the service of the electronic equipment. I am grateful to Professor S. Frederick Ravitz who kindly introduced me to the facilities of IMRD, where I prepared the samples. Finally, I would like to express my appreciation to Miss E. Kathy Williams, who kindly typed the first draft of this dissertation.

This work was done under the auspices of the University of Chile - University of California Exchange Program, with support from the U. S. Atomic Energy Commission through the Inorganic Materials Research Division of the Lawrence Radiation Laboratory.

REFERENCES

1. J. C. Slater, J. Appl. Phys. 39, 761 (1968).

2. C. Kittel, Introduction to Solid State Physics, 3d ed. (John Wiley & Sons, Inc., New York, 1966), Chap. 5.

3. K. P. Gupta, C. H. Cheng, and P. A. Beck, Phys. Rev. 133, A203 (1964).

4. A. M. Clogston, B. T. Matthias, M. Peter, H. J. Williams, E. Corenzwit, R. C. Sherwood, Phys. Rev. 125, 541 (1962).

5. E. E. Barton and H. Claus, Phys. Rev. 1B, 3741 (1970).

6. T. J. Hicks, B. Rainford, J. S. Kouvel, G. G. Low, and J. B. Comly, Phys. Rev. Letters 22, 531 (1969).

7. A. J. Freeman and R. E. Watson, Hyperfine Interactions in Magnetic Materials, in Magnetism (Academic Press, New York, 1965) Vol. II-A, p. 167.

8. R. E. Behringer, J. Phys. Chem. Solids 2, 209 (1957).

9. P. P. Craig, D. E. Nalge, W. A. Steyert, and R. D. Taylor, Phys. Rev. Letters 9, 12 (1962).

10. C. T. Wei, C. H. Cheng, and P. A. Beck, Phys. Rev. 122, 1129 (1961).

11. D. A. Shirley, S. S. Rosenblum, and E. Matthias, Phys. Rev. 170, 363 (1968).

12. J. Friedel, Canad. J. Phys. 34, 1190 (1956); J. Phys. Rad. 17, 27 (1956); Nuovo Cimento 8, Suppl. 2, 287 (1958).

13. P. W. Anderson, Phys. Rev. 124, 41 (1961).

14. P. A. Wolff, Phys. Rev. 124, 1030 (1961).

15. J. Kondo, Progr. Theoret. Phys. (Kyoto) 32, 37 (1964).

16. M. D. Daybell and W. A. Steyert, Rev. Mod. Phys. 40, 380 (1968).

17. M. F. Collins and G. G. Low, Proc. Phys. Soc. 86, 535 (1965).

18. J. W. Cable, E. O. Wollan, and H. R. Child, Phys. Rev. Letters 22, 1256 (1969).

19. E. L. Hahn, Phys. Rev. 80, 580 (1950).

20. M. H. Bancroft, Phys. Rev. B2, 182 (1970).

21. J. Korringa, Physica 16, 601 (1950).

22. A. Narath and H. T. Weaver, Phys. Rev. 175, 373 (1968).

23. Y. Obata, J. Phys. Soc. Japan 18, 1020 (1963).

24. T. Moriya, J. Phys. Soc. Japan 19, 681 (1964).

25. R. E. Walstedt, V. Jaccarino and N. Kaplan, J. Phys. Soc. Japan 21, 1843 (1966).

26. M. E. Rose, Elementary Theory of Angular Momentum (John Wiley & Sons, Inc., New York, 1957) p. 61.

27. E. U. Condon and G. H. Shortley, The Theory of Atomic Spectra (Cambridge University Press, London, 1964) p. 77.

28. C. Kittel, Quantum Theory of Solids (John Wiley & Sons, Inc., New York, 1964) p. 54.

29. Handbook of Operational Amplifier Applications, edited by Burr-Brown Research Corp. (Tucson, Arizona, 1963).

30. A. Abragam, The Principles of Nuclear Magnetism (Oxford University Press, London, 1962), p. 79.

31. Measurements, in The Radio Amateur's Handbook, 46th ed., edited by Doug De Maw, (American Radio Relay League, Newington, Conn., 1969), p. 557.

32. G. L. Samuelson and D. C. Ailion, Rev. Sci. Instr. 40, 676 (1969).

33. R. L. Streever and L. H. Bennett, Phys. Rev. 131, 2000 (1963).

34. J. N. Aubrun and L. D. Khoi, C. R. Acad. Sc. 263 B-249 (1966).

35. A. C. Gossard and A. M. Portis, Suppl. J. Appl. Phys. 31, 205 (1960).

36. W. B. Mims, Phys. Rev. 141, 499 (1966).

37. P. R. Locher and S. Geshwind, Phys. Rev. Letters 11, 333 (1963).

38. M. Kontani and J. Itoh, J. Phys. Soc. Japan 22, 345 (1966).

39. V. S. Shirley, Table of Nuclear Moments, in Hyperfine Structure and Nuclear Radiations, edited by E. Matthias and D. A. Shirley (North-Holland Publishing Co., Amsterdam, 1968).

40. J. I. Budnick and S. Skalski, Nuclear Magnetic Resonance in Some Magnetically Ordered Systems, in Hyperfine Interactions, edited by A. J. Freeman and R. B. Frankel, (Academic Press, New York, 1967).

41. R. H. Hammond and W. D. Knight, Phys. Rev. 120, 762 (1960).

42. A. M. Portis, Phys. Rev. 104, 584 (1956).

43. M. H. Bancroft, Nuclear Relaxation of Cu^{63} in Ni-Cu (Ph.D. thesis), UCRL-18461, September 1968.

44. E. R. Andrew and D. P. Tunstall, Proc. Phys. Soc. 78, 1 (1961).

45. W. W. Simmons, W. J. O'Sullivan, and W. A. Robinson, Phys. Rev. 127, 1168 (1962).

46. A. Narath, Phys. Rev. 162, 320 (1967).

47. F. Herman and S. Skillman, Atomic Structure Calculations (Prentice-Hall, Inc., N. J., 1963).

48. J. W. D. Connolly, Phys. Rev. 159, 415 (1967).

49. G. A. Burdick, Phys. Rev. 129, 138 (1963).

50. H. A. Mook, Phys. Rev. 148, 495 (1966).

51. A. G. Anderson and A. G. Redfield, Phys. Rev. 116, 583 (1959).

52. L. C. Davis and S. H. Liu, Phys. Rev. 163, 503 (1967).

53. E. I. Zornberg, unpublished.

54. J. C. Phillips, J. Appl. Phys. 39, 755 (1968).

55. G. Fischer, A. Herr, and A. J. P. Meyer, J. Appl. Phys. 39, 545 (1968).

56. A. J. Freeman and R. E. Watson, Hyperfine Interactions in Magnetic Materials, in Magnetism, Vol. 2-A, edited by G. T. Rado and M. Suhl, (Academic Press, N. Y., 1965).

57. J. W. Cable and H. R. Child, Phys. Rev. 1B, 3809 (1970).

58. W. Marshall, J. Phys. C1, 88 (1968).

59. J. Crangle and W. R. Scott, J. Appl. Phys. 36, 921 (1965).

60. M. F. Collins and G. G. Low, Proc. Phys. Soc. 86, 535 (1965).

61. J. B. Comly, T. M. Holden, and G. G. Low, J. Phys. C. (Proc. Phys. Soc.) 1, 458 (1968).

62. J. W. Cable, J. O. Wollan, and H. R. Child, Phys. Rev. Letters 22, 1256 (1969).

63. M. B. Stearns, J. Appl. Phys. 36, 913 (1965).

64. R. C. LaForce, S. F. Ravitz, and G. F. Day, Phys. Rev. Letters 6, 226 (1961).

65. P. C. Riedi and R. G. Scurlock, J. Appl. Phys. 39, 124 (1968).

66. H. Danan, A. Herr, and A. J. P. Meyer, J. Appl. Phys. 39, 669 (1968).

APPENDIX

Here we give a listing of the computer programs. They are written in Fortran II language and were used in an IBM 1620 computer with disc storage.

The programs are self-explanatory; we shall add now a few remarks.

The calibration table in subroutine REDUC4 was obtained as the output of the receiver system when the input was varied in steps of 1 dB. There was a precision attenuator connected between the signal generator and the receiver input.

Program EFEX2 calculates the parameters M_o, β, and T_1 in a least-squares fit. The equation is:

$$M(t) = M_o[1 - \beta \exp(-t/T_1)].$$

If M_o were known, it would be very simple to get β and T_1 by taking logarithms:

$$\ell n\,[1 - M(t)/M_o] = \ell n\,\beta - t/T_1$$

which is a linear relationship. This is done in subroutine RQZ. After solving for β and T_1, we get a transcendental equation for M_o. It is solved in program EFEX2 by the regula falsi method.

```
CCCC  PROGRAMS EFEX PLUS EFEX2 READ DATA AND MAKE  A LEAST SQUARES
CCCC  CALCULATION OF T1, MO AND BETA, IN M(T) =  MO(1-BETA*EXP(-T/T1))
CCCC  DATA POINTS ARE T AND M(T)
      DIMENSION TITLE(80),TIME(20),COUNT(20),VOLTS(20), EMM(20)
      COMMON SCALE, ENE3,ENE4, ENE2, EMO, EMOO, NN, MM
      COMMON TITLE, TIME, COUNT, VOLTS, EMM,TEMP, FMAG, NATEN
      PRINT 99
   99 FORMAT (1H1,5X,12HPROGRAM EFEX  )
CCCC  READ 4 CARDS OF ALPHANUMERIC DATA (HEADING)
      READ 100, TITLE
  100 FORMAT (20A4)
      PRINT 101, TITLE
  101 FORMAT (1H ,20A4)
CCCC  TEMP IS ABSOLUTE TEMPERATURE IN *K) FMAG IS MAGNETIC FIELD IN
CCCC  GAUSS.  NATEN IS SETTING OF ATTENUATOR IN DB.
      READ 102, TEMP, FMAG, NATEN
  102 FORMAT (2F10.0,I2)
      PRINT 130, TEMP, FMAG, NATEN
  130 FORMAT (1H ,///10X,6HTEMP =,F7.2,3H *K,10X,13HMAGN. FIELD =,F7.0,6
     1H GAUSS,15X,9HATTEN. =  ,I2,3H DB /)
CCCC  MEASUREMENT REPEATED ENE2 TIMES. FOR CALIBRATION, A 100 KHZ SIGNAL
CCCC  GIVES ENE3 COUNTS AFTER ENE4 MEASUREMENTS
CCCC  SCALE OF V. TO F. CONVERTER) FULL SCALE OUTPUT IS 100 KHZ.
      READ 104, SCALE, ENE3, ENE4, ENE2, EMO
  104 FORMAT (5F10.0)
      F = SCALE*ENE4/(ENE2*ENE3)
      EMOO = F*EMO
      PRINT 105, SCALE, ENE3, ENE4
  105 FORMAT (1H ,///10X,7HSCALE =,F5.1,17H V.  CALIBRATION,,F7.0,13H CO
     1UNTS AFTER, F6.0, 5HTIMES /)
      PRINT 106, ENE2, EMO
  106 FORMAT (1H ,5X,20HMEASUREMENT REPEATED,F7.0,5HTIMES,15X,4HMO =,
     1  F9.0//)
CCCC  SUBROUTINE REDUC4 CORRECTS FOR LACK OF LINEARITY OF THE SYSTEM.
      CALL REDUC4 (EMOO,C)
C
      DO 1 NN=1,20
      READ 108, TIME(NN),COUNT(NN)
  108 FORMAT (2F10.0)
      IF (TIME(NN)) 1,70,1
    1 CONTINUE
C
   70 CONTINUE
C
C
      DO 62 MM=NN,20
CCCC  TIME(NN) AND COUNT(NN) ARE THE DATA POINTS.  TWO BLANK CARDS AT THE END.
CCCC  END. IF THERE IS A BLANK CARD BETWEEN DATA CARDS, THEN ALL THE
CCCC  CARDS AFTER THE BLANK CARD ARE READ AND PRINTED, BUT NOT USED
CCCC  FOR THE COMPUTATION(
      READ 108,TIME(MM),COUNT(MM)
      IF (TIME(MM)) 62,72,62
   62 CONTINUE
C
   72 CONTINUE
      MM = MM-1
      NN = NN-1
      EN = NN
C
      DO 61 J=1,MM
      VOLTS(J) = F*COUNT(J)
      CALL REDUC4 (VOLTS(J),EMM(J))
      EMM(J) = EMM(J)/C
   61 CONTINUE
C
      CALL LINK (EFEX2)
      END
*** (END LISTING)
```

```
CCCC  PROGRAM EFEX2.   CONTINUATION OF EFEX.
      DIMENSION TITLE(80),TIME(20),COUNT(20),VOLTS(20), EMM(20)
      DIMENSION Y(20), ZETA(8), X(8)
      COMMON SCALE, ENE3,ENE4, ENE2, EMO, EM00, NN, MM
      COMMON TITLE, TIME, COUNT, VOLTS, EMM,TEMP, FMAG, NATEN
      PRINT 115
  115 FORMAT (1H ,20X,15HTABULATION OF Z   / )
      PRINT 118
  118 FORMAT(1H ,20X,2HMO,15X,1HR,15X,1HQ,15X,1HZ,9X,9HSTD. DEV.  /  )
      START = 1.2
      DELTA = .01
CCCC SENSE SWITCH 3 ON ALLOWS TO CHANGE START AND DELTA.
      IF (SENSE SWITCH 3) 36,400
   36 CONTINUE
      ACCEPT 98, START, DELTA
   98 FORMAT (2F10.0)
  400 CONTINUE
      EM00 = START
      L = 1
CCCC  SUBROUTINE RQZ CALCULATES PARAMETERS, RR @ 1/T1, QQ = LOGE(BETA)
CCCC  IN A LEAST SQUARES FIT( FOR A GIVEN VALUE OF MO
      CALL RQZ (TIME,EMM,NN,EM00,Y,RR,QQ,ZZ,SS)
      ZETA(1) = ZZ
      X(1) = EM00
C
      DO 33 I=1,40
      AI = I
      EM00 = START-DELTA*AI
      CALL RQZ (TIME,EMM,NN,EM00,Y,RR,QQ,ZZ,SS)
      PRINT 119, I, EM00, RR, QQ, ZZ, SS
      IF (L-7) 41,41,33
   41 CONTINUE
      IF (ZZ*ZETA(L)) 38,38,35
   38 CONTINUE
      X(L+1) = EM00
      ZETA(L+1) = ZZ
      L = L+2
      IF (L-7) 35,35,33
   35 CONTINUE
      X(L) = EM00
      ZETA(L) = ZZ
   33 CONTINUE
C
CCCC  LL GIVES THE CHOICE OF ONE MINIMUM OF SS)
      ACCEPT 777, LL
  777 FORMAT (I1)
      LL = 2*LL-1
CCCC  SOLVE EQUATION Z(MO) @ 0. BY REGULA FALSI METHOD.
      PRINT 117
  117 FORMAT (1H ,///1H , 30HSOLUTION OF EQUATION Z(MO) = 0     /  )
      PRINT 116, LL,X(LL),ZETA(LL),X(LL+1),ZETA(LL+1)
  116 FORMAT (1H ,10X,I3,2(6X,F7.4,3X,E12.5) / )
      PRINT 118
C
      DO 37 II=1,500
      TEMP2 = (X(LL+1)*ZETA(LL)-X(LL)*ZETA(LL+1))/(ZETA(LL)-ZETA(LL+1))
      IF (ABSF(1.-(TEMP2/TEMP3))-1.E-7) 87,22,22
   22 CONTINUE
CCCC  IF CONVERGENCE IS TOO SLOW, TURN SENSE SWITCH 3 ON AND START
CCCC  AGAIN WITH NEW TABULATION
      IF (SENSE SWITCH 3) 36,23
```

```
   23 CONTINUE
      TEMP3 = TEMP2
      CALL RQZ (TIME,EMM,NN,TEMP2, Y,RR,QQ,ZZ,SS)
      PRINT 119, II,TEMP2,RR,QQ,ZZ,SS
  119 FORMAT (1H ,10X,I3,4X,F10.7,4(4X,E12.5))
      IF (ZZ*ZETA(LL)) 19,19,21
   19 CONTINUE
      ZETA(LL+1) = ZZ
      X(LL+1) = TEMP2
      GO TO 37
   21 ZETA(LL) = ZZ
      X(LL) = TEMP2
   37 CONTINUE
C
   87 CONTINUE
      X(LL) = TEMP2
      X(LL+1) = SS
      ZETA(LL) = -1./RR
      ZETA(LL+1) = EXPF (QQ)
      PRINT 120
  120 FORMAT (1H ,  /  )
      PRINT 99
   99 FORMAT (1H1,5X,12HPROGRAM EFEX  )
      PRINT 101, TITLE
  101 FORMAT (1H ,20A4)
      PRINT 130, TEMP,FMAG,NATEN
  130 FORMAT (1H ,///10X,6HTEMP =,F7.2,3H *K,10X,13HMAGN. FIELD =,F7.0,6
     1H GAUSS,15X,9HATTEN. =  ,I2,3H DB /)
      PRINT 105, SCALE, ENE3, ENE4
  105 FORMAT (1H ,///10X,7HSCALE =,F5.1,17H V.  CALIBRATION,,F7.0,13H CO
     1UNTS AFTER, F6.0, 5HTIMES /)
      PRINT 106, ENE2, EMO
  106 FORMAT (1H ,5X,20HMEASUREMENT REPEATED,F7.0,5HTIMES,15X,4HMO =,
     1  F9.0//)
      PRINT 109, ZETA(LL),ZETA(LL+1),X(LL),X(LL+1)
  109 FORMAT (1H ,4HT1 =,F10.3,10X,6HBETA =,F7.4,10X,4HMO =,F8.5,10X,16H
     1STD. DEVIATION = ,E11.4  /  )
      PRINT 107
  107 FORMAT(1H ,//4X,4HTIME,4X,6HCOUNTS,5X,5HVOLTS,7X,4HM(T),14X,
     1  7H1.-M/MO ,5X,5HTHEO.   /  )
C
      DO 301 J=1,NN
      RESEXP = 1.-EMM(J)/X(LL)
      RESTHE = ZETA(LL+1)*EXPF(-TIME(J)/ZETA(LL))
      PRINT 208, TIME(J),COUNT(J),VOLTS(J),EMM(J),RESEXP,RESTHE
  208 FORMAT (1H ,F8.1,F9.0,2F11.5,1X,10X,F8.5,4X,F8.5  )
  301 CONTINUE
C
      PRINT 120
      NN = NN+1
C
      DO 305 J=NN,MM
      RESEXP = 1.-EMM(J)/X(LL)
      RESTHE = ZETA(LL+1)*EXPF(-TIME(J)/ZETA(LL))
      PRINT 208, TIME(J),COUNT(J),VOLTS(J),EMM(J),RESEXP,RESTHE
  305 CONTINUE
      END
#### (END LISTING)
```

```
CCCC  SUBROUTINE REDUC4 GIVES THE CORRECTED VALUE OF THE SIGNAL. IT INTER-
CCCC  POLATES LINEARLY THE LOGARITHM OF THE SIGNAL.
CCCC  TABLE Y(I) IS CALIBRATION OF SYSTEM
      SUBROUTINE REDUC4 (YYY, XXX)
      DIMENSION Y(20)
CCCC  Y(I) ARE NUMBER OF COUNTS AFTER EN2 MEASUREMENS
      Y(1)  = 4400.
      Y(2)  = 3860.
      Y(3)  = 3411.
      Y(4)  = 3028.
      Y(5)  = 2690.
      Y(6)  = 2409.
      Y(7)  = 2138.
      Y(8)  = 1881.
      Y(9)  = 1659.
      Y(10) = 1445.
      Y(11) = 1260.
      Y(12) = 1105.
      Y(13) =  975.
      Y(14) =  860.
      Y(15) =  760.
      Y(16) =  664.
      Y(17) =  580.
      Y(18) =  505.
      Y(19) =  438.
      Y(20) =  375.
      EN2 = 100.
CCCC  FOR CALIBRATION, A 100 KHZ SIGNAL GIVES EN3 COUNTS AFTER EN4 TIMES
      EN3 = 99884.
CCCC  SCALE IS 10 V
      EN4 = 1000.
      FF = 10.*EN4/(EN2*EN3)
C
      DO 69 J = 1,20
      Y(J) = FF*Y(J)
   69 CONTINUE
C
      VV = LOGF (YYY)
C
      DO 70 I = 1, 20
      IF (YYY-Y(I)) 70,71,71
   70 CONTINUE
C
      I = 20
   71 PI = I-1
      VI = LOGF (Y(I))
      VIM = LOGF (Y(I-1))
      U = (VIM*PI - VI*(PI-1.) - VV)* 0.05/(VI-VIM)
      XXX = Y(1)*EXPF (2.302585*U)
      RETURN
      END
#### (END LISTING)
```

```
CCCC  SUBROUTINE ROZ CALCULATES PARAMETERS, RR @ 1/T1, QQ = LOGE(
CCCC  IN A LEAST SQUARES FIT( FOR A GIVEN VALUE OF MO
      SUBROUTINE ROZ (T,EM,N,EMO,Y,R,Q,Z,S)
      DIMENSION T(20), EM(20), Y(20)
      SMYT = 0.
      SMY = 0.
      SMT = 0.
      SMTSQ = 0.
      SMYM = 0.
      SMTM = 0.
      SMM = 0.
      SMYSQ = 0.
      EN = N
C
      DO 60 J = 1,N
      A = 1.-EM(J)/EMO
      Y(J) = ABSF(A)
      Y(J) = LOGF (Y(J))
      SMYT = SMYT + (T(J)*Y(J))
      SMY = SMY + Y(J)
      SMT = SMT + T(J)
      SMTSQ = SMTSQ + T(J)*T(J)
      SMYSQ = SMYSQ + Y(J)*Y(J)
      SMYM = SMYM + Y(J)/A
      SMTM = SMTM + T(J)/A
      SMM = SMM + 1./A
   60 CONTINUE
C
      A = EN*SMTSQ - SMT*SMT
      R = (EN*SMYT-SMY*SMT)/A
      Q = (SMY*SMTSQ-SMT*SMYT)/A
      Z = SMYM - R*SMTM - Q*SMM
      A = SMYSQ - R*SMYT - Q*SMY
      S = SQRTF (A/EN)
      RETURN
      END
#### (END LISTING)
```

```
CCCC  PROGRAM HF CALCULATES THE AVERAGE OF 1/R**3 BY NUMERICAL
CCCC  INTEGRATION. WAVE FUNCTIONS TAKEN FROM HERMAN AND SKILLMAN'S TABLES.
      DIMENSION TITLE(20)
      DIMENSION P(11), X(11)
      PRINT 99
   99 FORMAT (1H1,  88HCALCULATON OF THE AVERAGE, ((1/R**3)), BY NUMERIC
     1AL INTEGRATION, USING SIMPSON RULE,          )
      PRINT 98
   98 FORMAT (1H ,55HFOR AN ORBITAL TAKEN FROM HERMAN AND SKILLMAN'S TABLES
     1LES     // )
CCCC  READ ONE CARD WITH ALPHANUMERIC DATA (HEADING)
      READ 100, TITLE
  100 FORMAT (20A4)
      PRINT 101, TITLE
  101 FORMAT (1H ,20A4  ///)
      AREA1 = 0.
      AREA2 = 0.
CCCC  Z = NZ = ATOMIC NUMBER
      READ 22,NZ
   22 FORMAT (I3)
      Z = NZ
CCCC  P(I) IS THE VALUE FROM THE WAVE FUNCTION TABLE FOR POINT X(I))
CCCC  THEY ARE READ IN GROUPS OF 11. THE FIRST PINT IN A GROUP IS THE
CCCC  REPETITION OF THE LAST POINT OF THE PREVIOUS GROUP.
C
      DO 1 K=1,20
      READ 2, X(1), DELX
    2 FORMAT (2F10.0)
CCCC  A BLANK CARD IS USED TO STOP READING DATA CARDS.
      IF (DELX) 7,8,7
    7 CONTINUE
      READ 13, P
   13 FORMAT (11F7.4)
C
      DO 12 I=2,11
      T = I-1
      X(I) = X(1) + T*DELX
   12 CONTINUE
C
      PRINT 3, X
    3 FORMAT (1H ,11(F6.2,4X))
      PRINT 4, P
    4 FORMAT (1H , 1X, 11(F7.4,3X))
C
      DO 5 J=1,11
      P(J) = P(J)*P(J)
    5 CONTINUE
C
CCCC  SUBROUTINE SUPER INTEGRATES BY SIMPSON'S RULE
      CALL SUPER(AR,P,DELX)
C
      AREA1 = AREA1 + AR
      DO 6 J=1,11
      P(J) = P(J)/(X(J)*X(J)*X(J))
    6 CONTINUE
C
      CALL SUPER (AR,P,DELX)
      AREA2 = AREA2 + AR
      PRINT 9, AREA1, AREA2
    9 FORMAT (1H ,10X,17HSUM (P**2*DELX) =  ,E12.5,10X,22HSUM (P**2*DELX
     1/X**3) =    ,E12.5   /)
```

```
    1 CONTINUE
C
    8 CONTINUE
      XMU = .88534138*(Z**(-1./3.))
      PRINT 32
   32 FORMAT (1H , // )
      PRINT 30, XMU
   30 FORMAT (1H ,10X,4HMU =   , E12.6 /  )
CCCC  AREA1 CHECKS NORMALIZATION OF THE WAVEFUNCTION.
      AREA1 = AREA1*XMU
CCCC  AREA2 IS MEASURED IN ATOMIC UNITS.
      AREA2 = AREA2/(XMU*XMU)
CCCC  AREA3 IS MEASURED IN CM-3
      AREA3 = AREA2*1.E24/(.529173**3.)
      PRINT 31, AREA1, AREA2, AREA3
   31 FORMAT (1H ,10X, 14HNORMALIZATION,  F7.4,15X,21HAVERAGE, ((1/R**3)
     1) = F9.4, 15X, E12.5,5H CM-3 )
      END
#### (END LISTING)
```

```
CCCC  SUBROUTINE SUPER INTEGRATES BY SIMPSON'S RULE
      SUBROUTINE SUPER (A,Y,DX)
      DIMENSION Y(11)
      EVEN = 0.
      ODD = 0.
C
      DO 15 J=2,10,2
      EVEN = EVEN + Y(J)
   15 CONTINUE
C
      DO 16 J=3,9,2
      ODD = ODD + Y(J)
   16 CONTINUE
C
      A = (Y(1)+4.*EVEN+2.*ODD+Y(11))*DX/3.
      RETURN
      END
#### (END LISTING)
```

Table I. Values of the coefficient $A(|m_1|,|m_2|,|m_3|)$ in the integral:
$\int Y_{2,m_1} Y_{2,m_2} Y_{2,m_3} \, d\Omega = \delta_{m_1,m_2+m_3} \, A(|m_1|,|m_2|,|m_3|)$

m_1	m_2	m_3	$A(\|m_1\|,\|m_2\|,\|m_3\|)$
0	0	0	$\frac{1}{7}\sqrt{\frac{5}{\pi}}$
1	1	0	$\frac{1}{14}\sqrt{\frac{5}{\pi}}$
2	2	0	$\frac{-1}{7}\sqrt{\frac{5}{\pi}}$
2	1	1	$\frac{1}{7}\sqrt{\frac{3}{2}}\sqrt{\frac{5}{\pi}}$

Table II. Cable and Child's results,[57] magnetic moments at 0°K of Ni-Pd alloys obtained by Bragg scattering and diffuse scattering of polarized neutrons.

	μ_{Ni}		μ_{Pd}	
at.% Pd	Bragg	Diffuse	Bragg	Diffuse
25	0.84 ± 0.02	0.81 ± 0.01	0.15 ± 0.11	0.00 ± 0.03
50	0.94 ± 0.04	1.02 ± 0.01	0.25 ± 0.06	0.17 ± 0.01
71	1.09 ± 0.08	1.13 ± 0.05	0.22 ± 0.06	0.20 ± 0.02
92	1.06 ± 0.12	1.28 ± 0.05	0.14 ± 0.02	0.07 ± 0.01

FIGURE CAPTIONS

Fig. 1. Slater-Pauling diagram. Average magnetic moments per atom as a function of the electron concentration, for transition metal binary alloys. From Kittel, Introduction to Solid State Physics, 3rd edition.

Fig. 2. Block diagram of the apparatus.

Fig. 3. Diagram of the receiver.

Fig. 4. Diagram of the connection of the sample coil.

Fig. 5. Diagram of the tuning operation.

Fig. 6. Simplified scheme of the boxcar integrator.

Fig. 7. Simplified scheme of the digital integrator.

Fig. 8. Pulse sequence for the transmitter and the averager.

Fig. 9. Resonant frequency vs external magnetic field.
o For Ni^{61} in Ni sponge, according to Bancroft[20] (left scale)
■ for Pd^{106} in Ni-Pd, our measurements (right scale).
Straight line is the theoretical response of single-domain spherical particles with a 2.3 kG demagnetizing field.

Fig. 10. Non-exponential recovery of the magnetization due to incomplete saturation.

Fig. 11. Spin-lattice relaxation in Ni metal. Annealed sample.

Fig. 12. Spin-lattice relaxation in different situations. Ni metal samples.
(a) long comb, produces heating of the sample;
(b) non-annealed sample;
(c) same as in Fig. 11, but at different scale.

Fig. 13. Density of states vs energy for the impurity levels. Spin up and spin down are separated. Nine different possibilities are considered.

Fig. 14. Magnetic moment in Bohr magneton units around a Pd atom in a dilute Ni-Pd alloy, 2 at.% concentration.

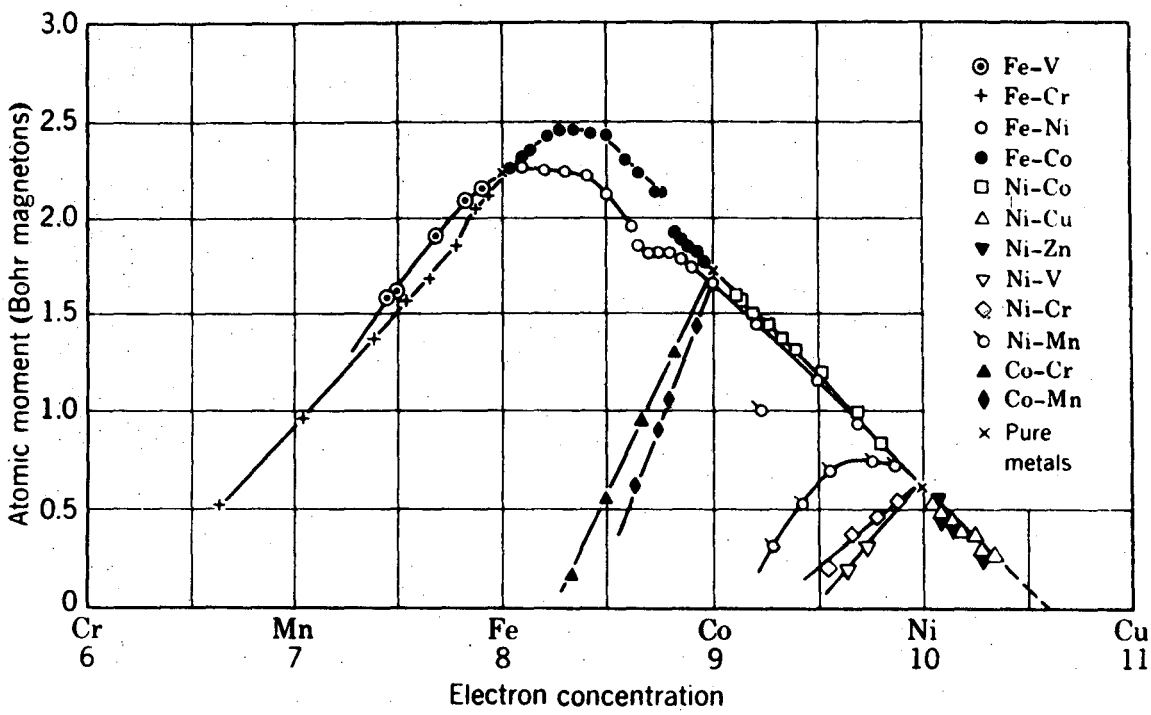

Figure 1

XBL 7011-7056

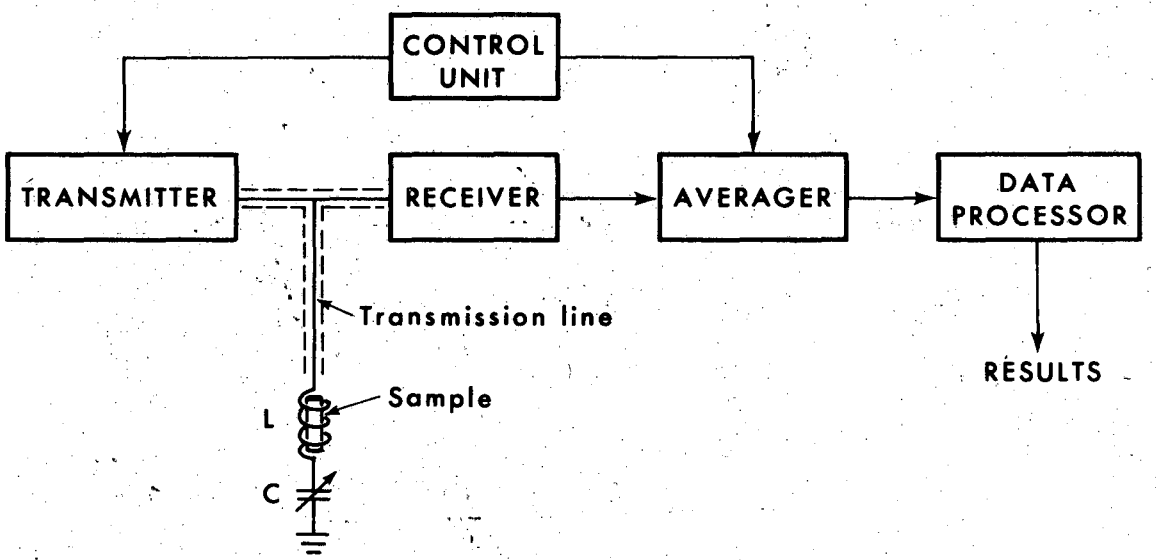

Figure 2

XBL 7011-7057

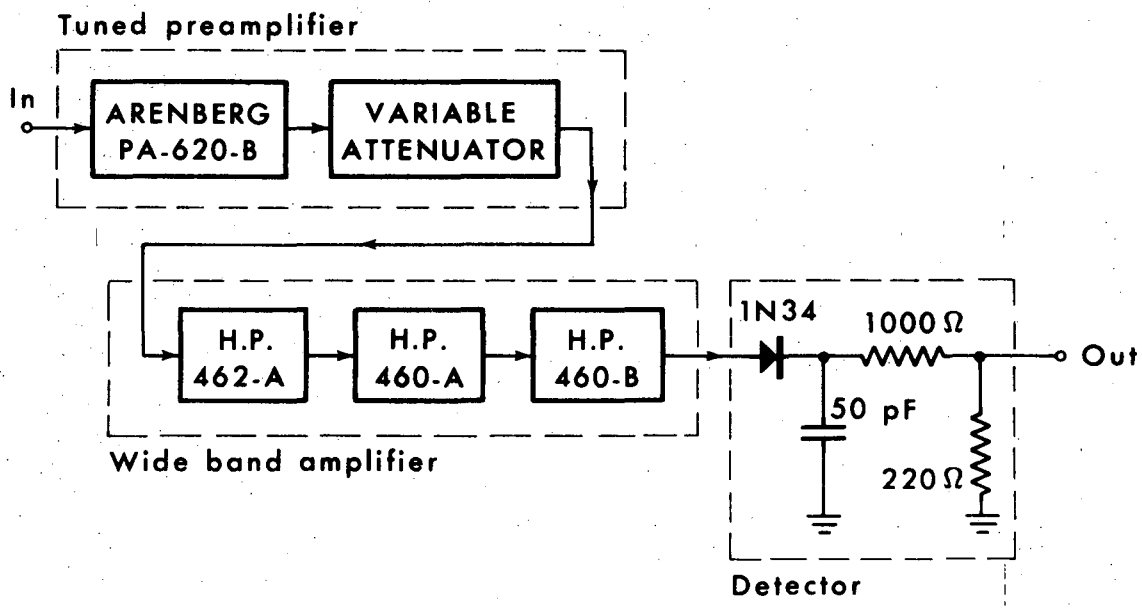

Figure 3

XBL 7011-7058

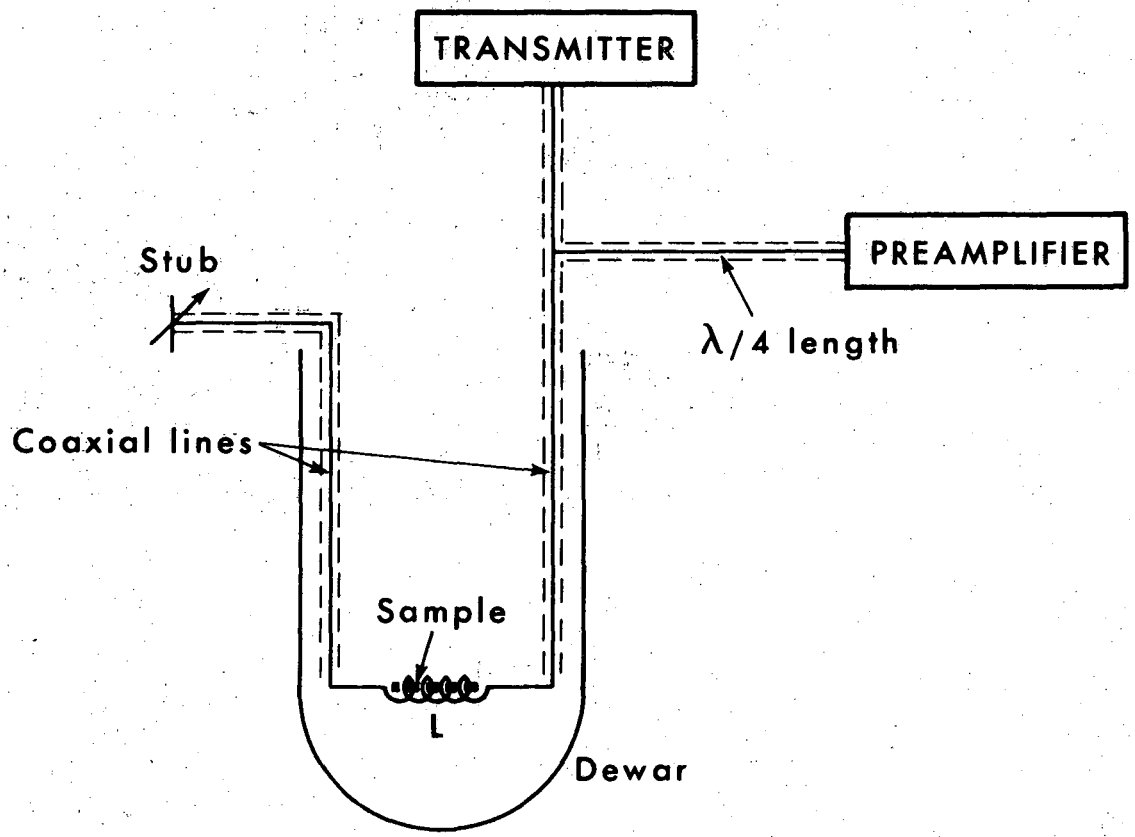

Figure 4

XBL 7011-7059

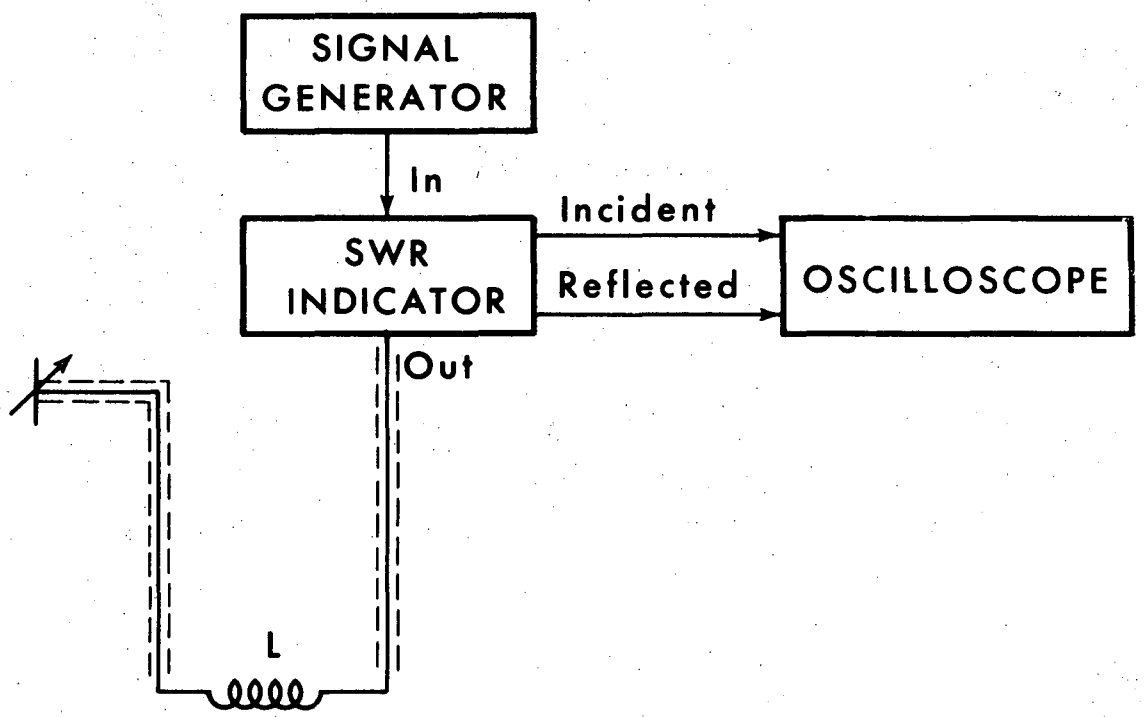

Figure 5

XBL 7011-7060

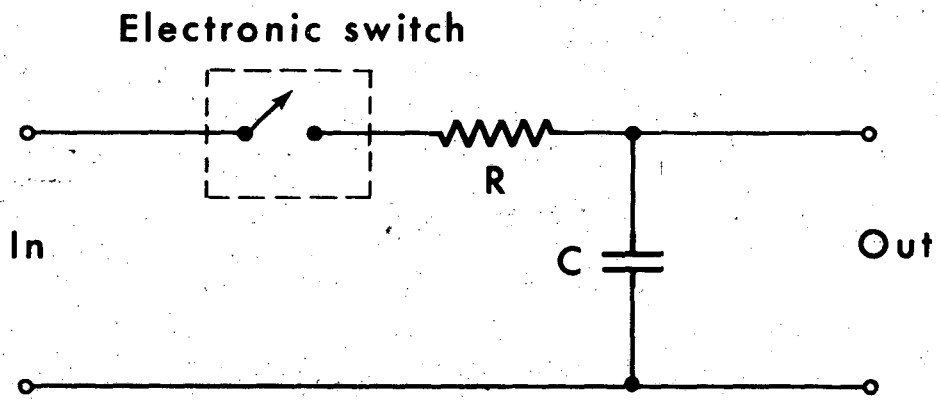

Figure 6

XBL 7011-7061

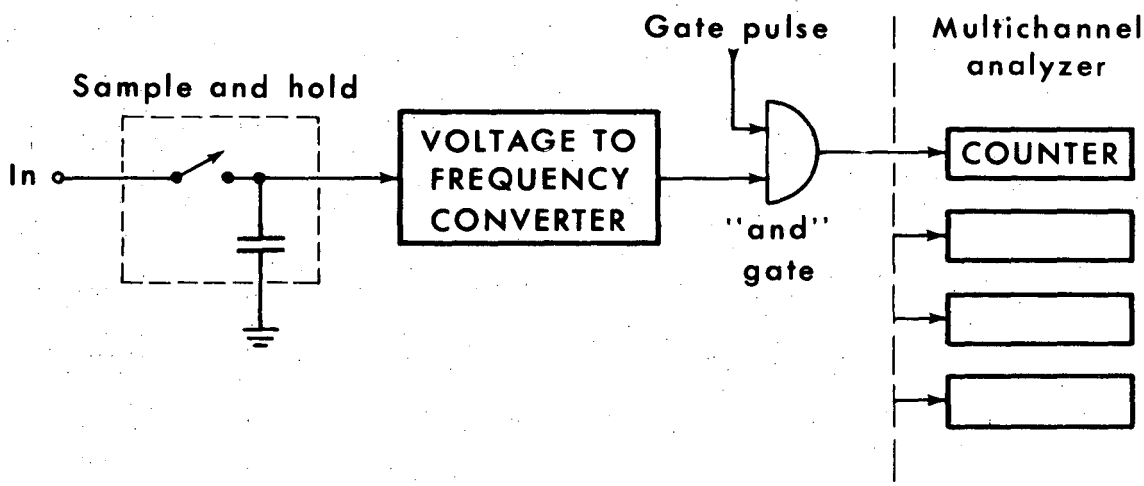

Figure 7

XBL 7011-7062

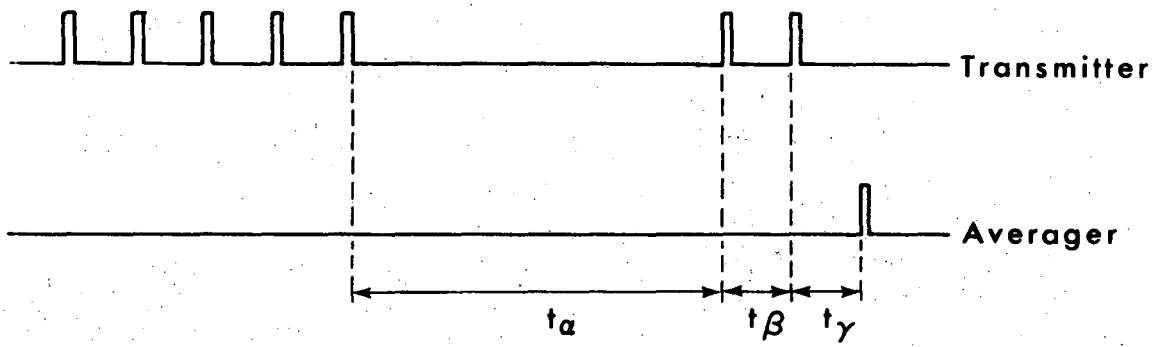

Figure 8

XBL 7011-7063

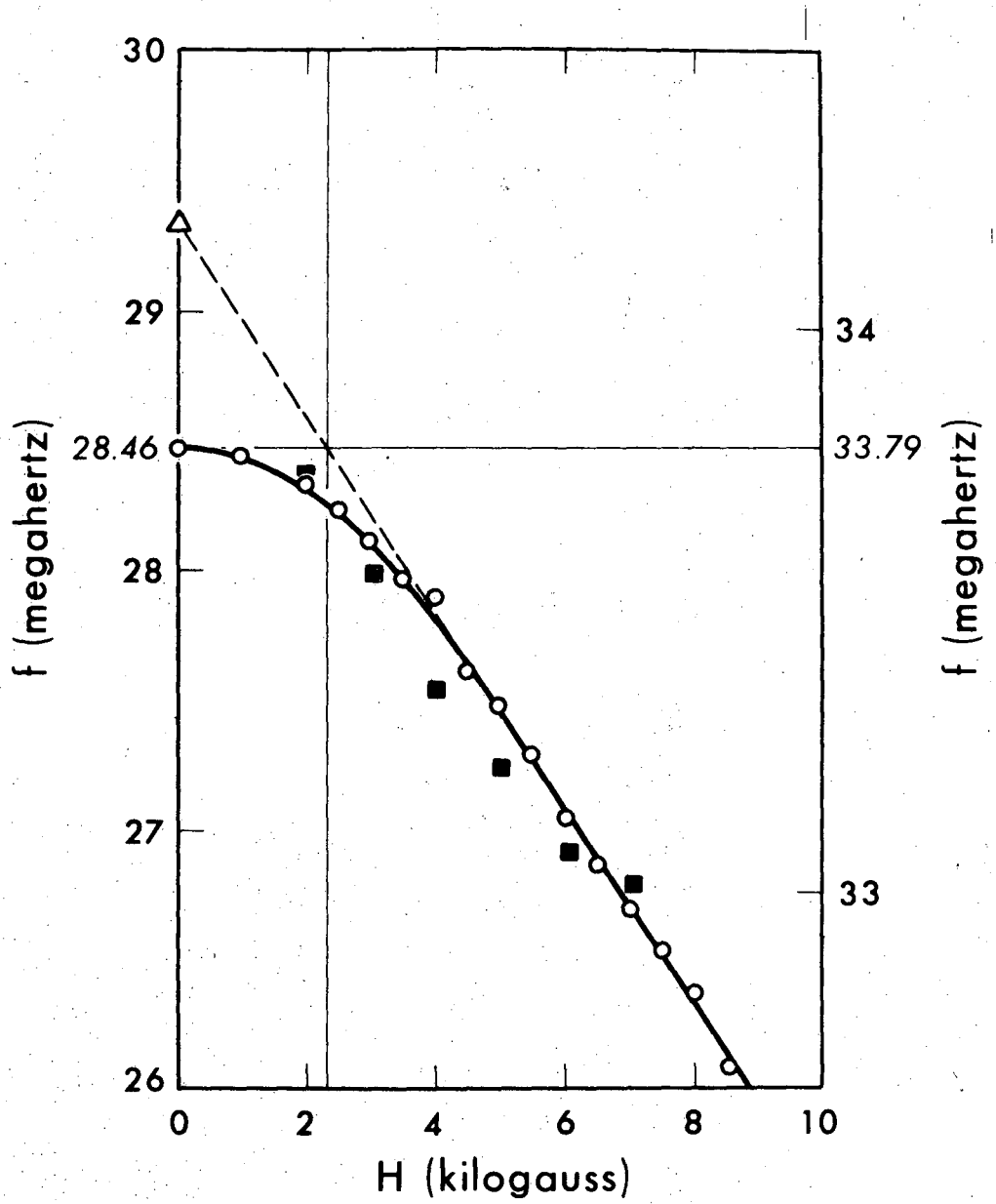

Figure 9

XBL 7011-7064

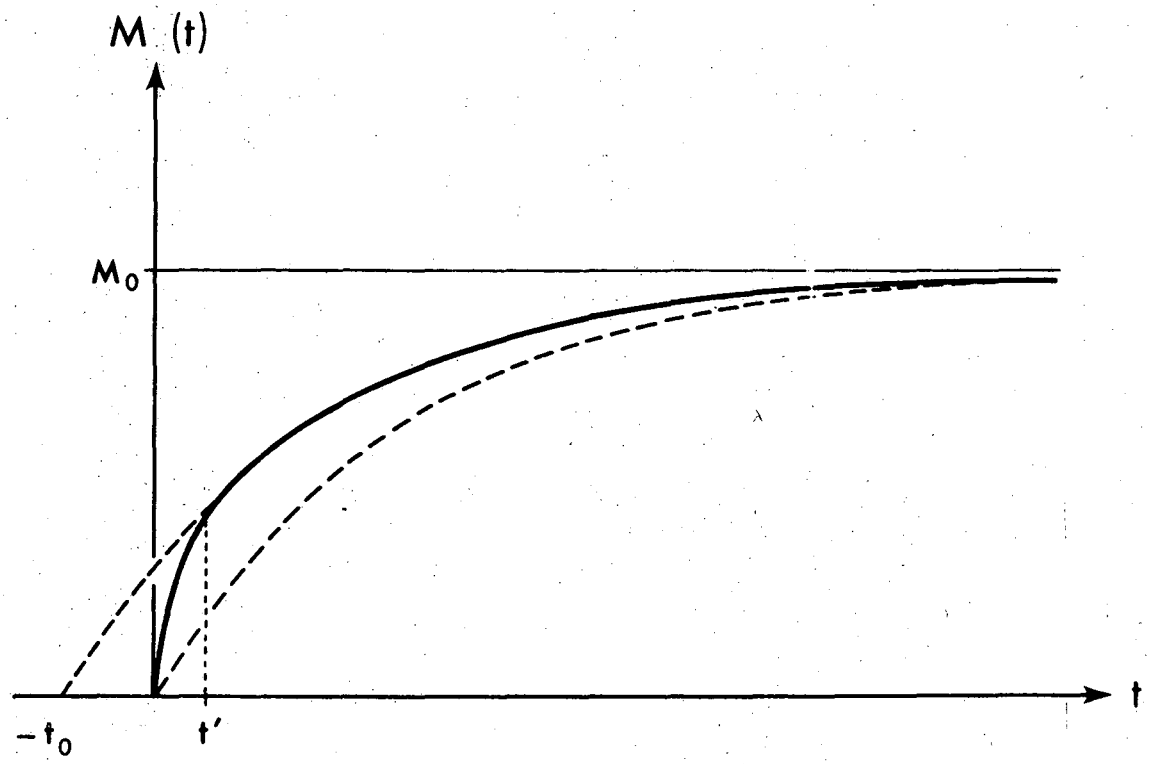

Figure 10

XBL 7011-7065

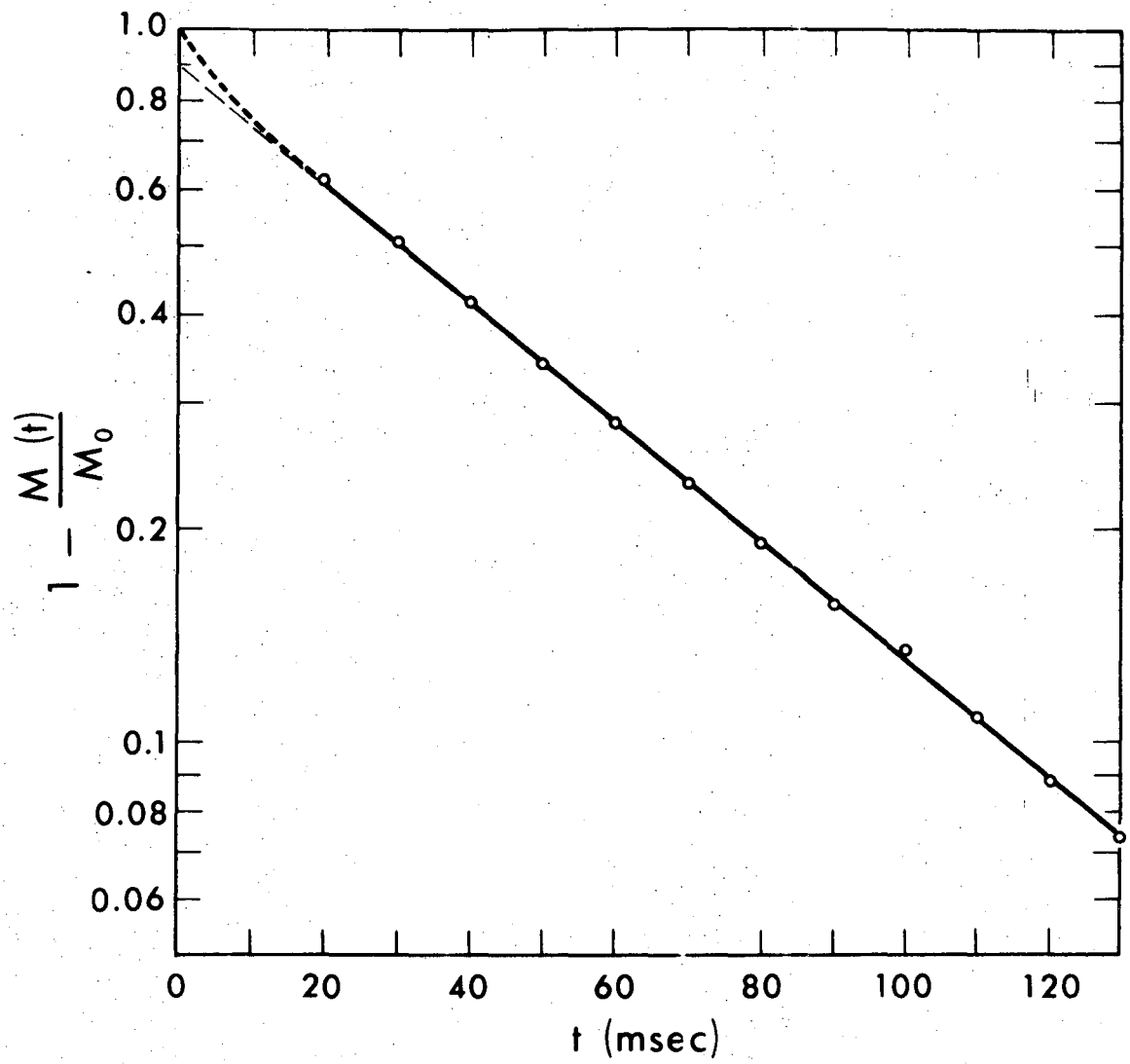

XBL 7011-7066

Figure 11

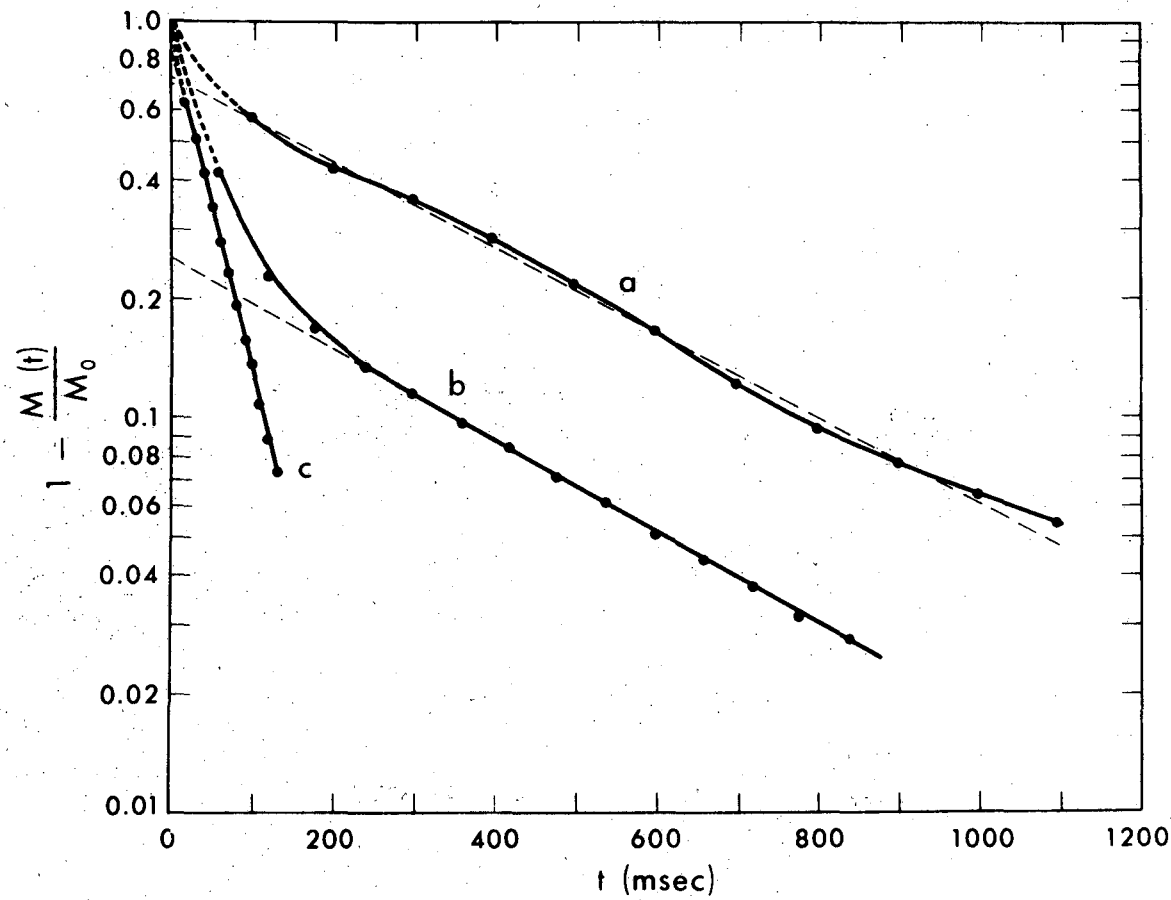

Figure 12

XBL 7011-7067

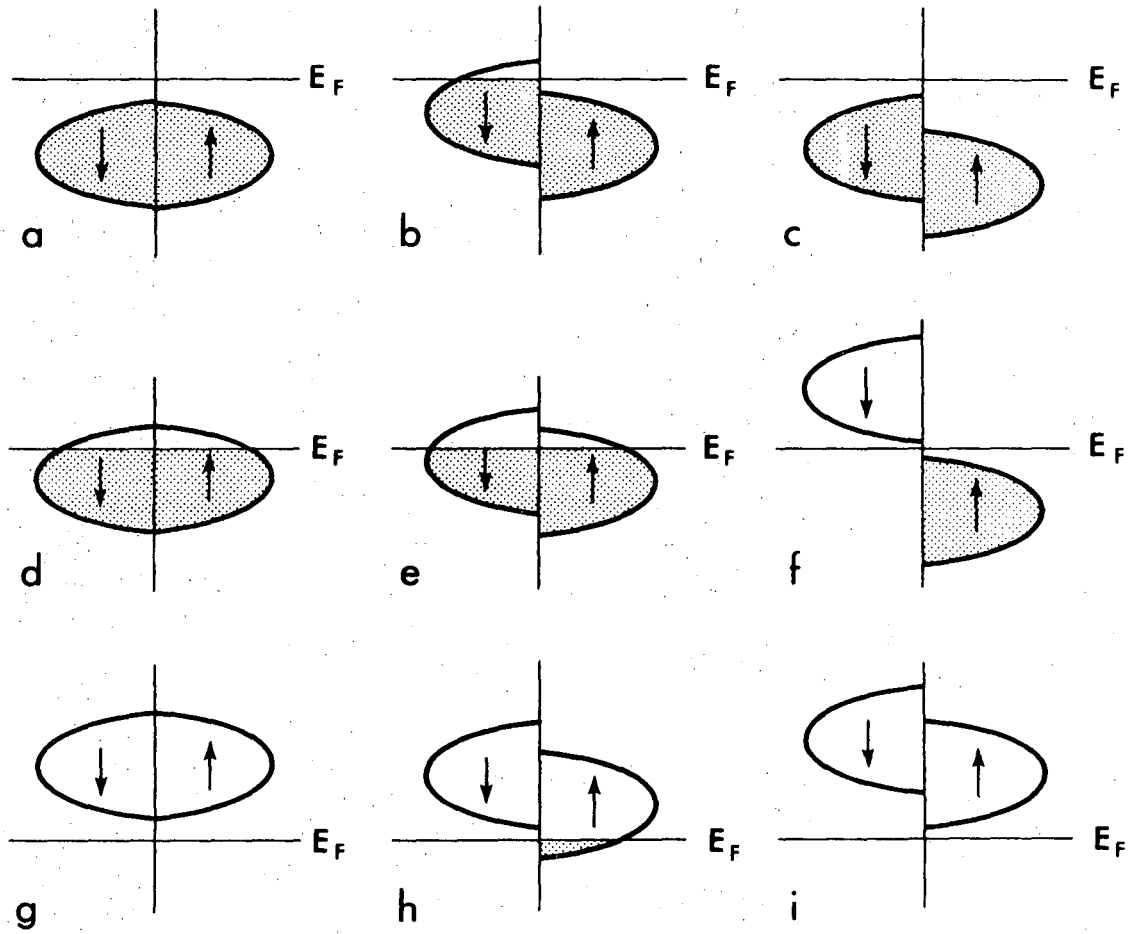

Figure 13

XBL 7011-7068

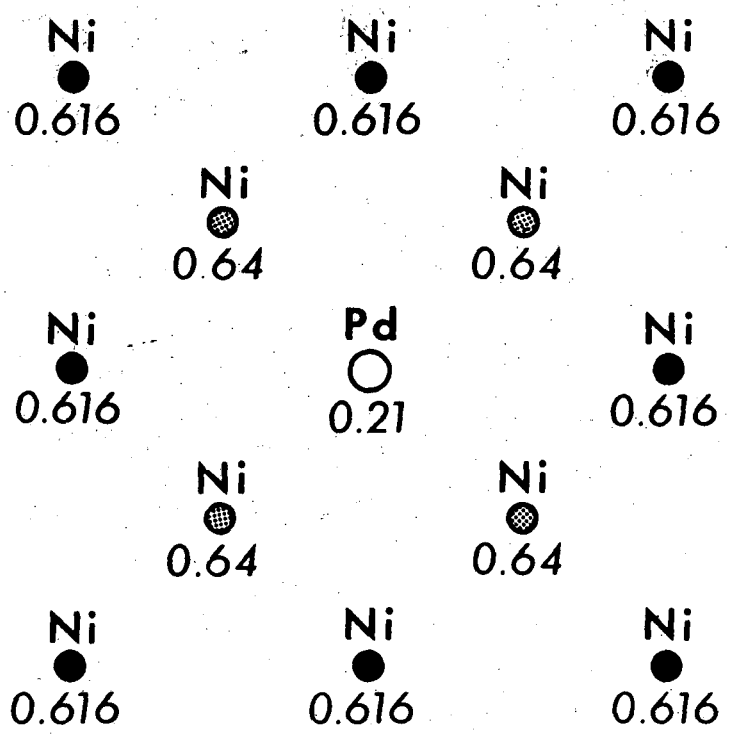

Figure 14

XBL 7011-7093

TECHNICAL INFORMATION DIVISION
LAWRENCE RADIATION LABORATORY
UNIVERSITY OF CALIFORNIA
BERKELEY, CALIFORNIA 94720